Synthesis of quinoline-carbaldehyde derivatives as novel inhibitors for leishmanial methionine aminopeptidase 1

Saleem Yousuf Bhat, Peddapaka Jagruthi, Angapelly Srinivas, Mohammed Arifuddin, Insaf Ahmed Qureshi

PII: S0223-5234(19)31012-8

DOI: https://doi.org/10.1016/j.ejmech.2019.111860

Reference: EJMECH 111860

To appear in: *European Journal of Medicinal Chemistry*

Received Date: 12 July 2019

Revised Date: 30 October 2019

Accepted Date: 5 November 2019

Please cite this article as: S.Y. Bhat, P. Jagruthi, A. Srinivas, M. Arifuddin, I.A. Qureshi, Synthesis of quinoline-carbaldehyde derivatives as novel inhibitors for leishmanial methionine aminopeptidase 1, *European Journal of Medicinal Chemistry* (2019), doi: https://doi.org/10.1016/j.ejmech.2019.111860.

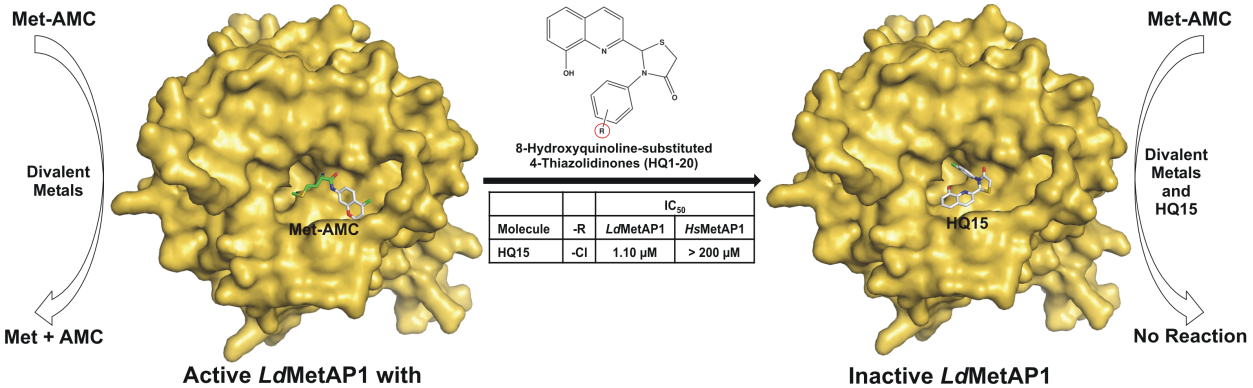

Synthesis of Quinoline-carbaldehyde derivatives as novel inhibitors for Leishmanial Methionine aminopeptidase 1

Saleem Yousuf Bhat[a], Peddapaka Jagruthi[b], Angapelly Srinivas[b], Mohammed Arifuddin[b] and Insaf Ahmed Qureshi[a]*

[a]Department of Biotechnology & Bioinformatics, School of Life Sciences, University of Hyderabad, Prof. C.R. Rao Road, Hyderabad 500046, India

[b]Department of Medicinal Chemistry, National Institute of Pharmaceutical Education and Research (NIPER), Hyderabad 500037, India.

*E-mail: insaf@uohyd.ac.in

Abstract

Leishmanial methionine aminopeptidase 1 (*Ld*MetAP1) is a novel antileishmanial target for its role in vital N-terminal methionine processing. After *Ld*MetAP1 expression and purification, we employed a series of biochemical assays to determine optimal conditions for catalysis, metal dependence and substrate preferences for this ubiquitous enzyme. Screening of newly synthesized quinoline-carbaldehyde derivatives in inhibition assays led to the identification of HQ14 and HQ15 as novel and specific inhibitors for *Ld*MetAP1 which compete with substrate for binding to the catalytic active site. Both leads bind *Ld*MetAP1 with high affinity and possess druglikeness. Biochemical studies suggested HQ14 and HQ15 to be comparatively less effective against purified *Hs*MetAP1 and showed no or less toxicity. We further show selectivity and inhibition of lead inhibitors is sensed through a non-catalytic Thr residue unique to *Ld*MetAP1. Finally, structural studies highlight key differences in the binding modes of HQ14 and HQ15 to *Ld*MetAP1 and *Hs*MetAP1 providing structural basis

for differences in inhibition. The study demonstrates the feasibility of deploying small drug like molecules to selectively target the catalytic activity of *Ld*MetAP1 which may provide an effective treatment of leishmaniasis.

Keywords

Leishmania donovani; Methionine aminopeptidase 1; Quinoline-carbaldehyde derivatives; Drug discovery

1. Introduction

Leishmaniasis is a major parasitic burden after malaria and appears in three major forms - visceral (also known as kala-azar and the most severe form), cutaneous (commonest form), and mucocutaneous form. Visceral form is often referred to as the disease of the poor and is associated with malnutrition, bad housing, population displacement and weak immune system. This disease is also connected to environmental changes, rampant urbanization and is caused by the dimorphic parasites of genus *Leishmania* which are disseminated into mammalian hosts through the bite of sandfly (http://www.who.int/mediacentre/factsheets/fs375/en/). The major symptoms of leishmaniasis include ulcerative skin lesions, fever, low RBC count, enlargement of spleen and liver which makes it life-threatening. Nearly one million new cases and about 30,000 deaths are reported annually in over 80 countries around the globe [1]. Absence of any significant vaccination accompanied with the reports of toxicity [2] and resistance against the current line of antileishmanials [3], there is a pressing need to identify newer molecular targets for therapeutic intervention against leishmaniasis.

Aminopeptidases are metal dependent exopeptidases that cleave amino acids from the N-terminal end in proteins and peptides [4]. The critical roles played by these enzymes in

nutrient acquisition [5] and the maintenance of protein turnover [6] makes them vital. Methionine aminopeptidases (MetAPs) remove initiator methionine from the N-terminus of nascent polypeptides either co-translationally or post-translationally [7-8] to enable necessary post-translational modifications [4,9]. MetAPs are ubiquitous, highly conserved and require a divalent metal cofactor for activity [4,7,10]. These enzymes are often seen as Co(II) activated metallo-enzymes with a dinuclear metal binding active site surrounded by residues DDHEE [7,10,11]. Apart from Co(II), other divalent metal ions like Fe(II), Mn(II) and Mg(II) are major activators [12]. However, the physiological activator appears to be Fe(II) [13].

Methionine aminopeptidases are grouped into two categories: type I and type II MetAP based on the presence of an additional amino acid insertion of nearly 60 amino acids residues towards the catalytic domain in the C-terminus of type II MetAP [8,14]. Prokaryotes express only MetAP1 whose deletion is reported to be lethal [15]. Eukaryotes express both types of MetAPs and develop lethality if either one or both MetAP genes are deleted [16]. Therefore, MetAPs have received attention as molecular targets for drug discovery against parasitic diseases [17] and severe adversaries like cancer [18].

Our study reports the expression, purification and a detailed characterization of methionine aminopeptidase 1 from *L. donovani* (*Ld*MetAP1). We have also synthesized and screened a library of quinoline-carbaldehyde derivatives to find novel inhibitors for *Ld*MetAP1. Using molecular, biochemical, biophysical and computational approaches, we show key differences between *Ld*MetAP1 and *Hs*MetAP1 and explain their differential inhibition by quinoline-carbaldehyde derivatives. We finally come up with two lead compounds with high druglikeness that may guide the development of highly specific and potent inhibitors against *Ld*MetAP1 and find use to combat leishmaniasis.

2. Results

2.1 Identification of *Ld*MetAP1gene, homology modelling and protein purification

To find genes responsible for methionine excision in the genome of *L. donovani,* we searched for *Ld*MetAP genes that were homologous to *Hs*MetAP1. We found a copy of both classes of methionine aminopeptidases (MetAPs) encoded by all species of *Leishmania*. Amongst the two MetAPs, one belongs to MetAP2 class based on the presence of an extra C terminal insertion near the catalytic domain while as, other MetAP belongs to the MetAP1 class of methionine aminopeptidases. Both *Ld*MetAP1 and *Ld*MetAP2 show high homology to their respective human counterparts and display a two domain organisation which is typical of M24 aminopeptidases (Fig. 2A). The analysis of *Ld*MetAP1 sequence revealed this protein to be 392 residues with its approximate molecular weight poised at 43.20 kDa. Since full length *Ld*MetAP1 could not be purified, we removed the initial 60 amino acid residues from the *Ld*MetAP1 ORF from the N-terminal non-catalytic domain and expressed and purified a truncated functional 38 kDa *Ld*MetAP1. The truncation was done knowing that the neglected N-terminal 60 residues are far-off from the C-terminal catalytic domain and have no role in *Ld*MetAP1 catalysis.

A homology model of 38 kDa *Ld*MetAP1 was built and validated (Fig. 2B). RMSD differences between *Ld*MetAP1 and *Tb*MetAP1 were 0.2 Å asserting the two structures to be very similar due to high sequence homology and the same pita-bread fold organization. Furthermore, overlay of the modelled *Ld*MetAP1 and *Hs*MetAP1 showed RMSD converge to 0.51 Å suggesting high structural similarity between all MetAP1 enzymes. The secondary structural composition of *Ld*MetAP1 resembles more with *Tb*MetAP1 than *Hs*MetAP1. In fact, secondary as well as tertiary structures of *Ld*MetAP1 and *Tb*MetAP1 are highly redundant. Like *Tb*MetAP1, the active site of *Ld*MetAP1 is located in the pita-bread fold bearing two metal ions and surrounded by two large α-helices and two β-sheets (Fig. 2C).

The metal ions are indispensable for catalysis because of their role in the generation of a strong nucleophile to break the sessile peptide bond while acting on nascent polypeptides or peptide substrates. Even though *Ld*MetAP1 is somewhat symmetrical in nature, its catalytic site is asymmetrically located in the highly conserved N-terminal domain. Besides, sequence alignment highlighted the evolutionary conservation of *Ld*MetAP1 active site and high sequence conservation with all MetAP1 class enzymes including the *Hs*MetAP1 (Fig. 2D). High resemblance of *Ld*MetAP1 to *Hs*MetAP1 is also evident from the presence of zinc-finger motif in the N-terminal extension of both enzymes.

Recombinant *Ld*MetAP1 was amplified from the genomic DNA of *L. donovani* and cloned into the expression vector pET28a. After expression in *E. coli* BL21 (DE3) cells, *Ld*MetAP1 was purified to homogeneity by Ni-NTA affinity chromatography and gel filtration chromatography (Fig. 2E). Other recombinantly expressed proteins T291A (lanes 3 and 4 in Fig. 2E) and *Hs*MetAP1 (Fig. 2F) were purified in a similar fashion. The quality of all purified proteins was assessed by 10% (w/v) SDS-PAGE which demonstrated all proteins to be highly homogenous. Furthermore, comparative analysis of the *Ld*MetAP1 partition coefficient (k_{av}) with those of the standard set of proteins suggested this enzyme to be monomeric in solution (Fig. 2G).

2.2 Determination of secondary structure and thermal stability

CD spectroscopy was employed to determine the secondary structure content of *Ld*MetAP1 and establish whether the average secondary structure of this enzyme changes after mutating Thr291 to Ala. The results of Far-UV spectra showed all recombinant proteins expressed in properly folded form with *Ld*MetAP1 composed of 21% α-helices and 24% β-sheets and T291A carrying 17% α-helices and 29% β-sheets (Fig. 3A). Therefore, T291A had slightly lesser α-helices and more β-sheets than *Ld*MetAP1. Heat denaturation assays in the

temperature range of 293 to 380 K indicated both *Ld*MetAP1 and T291A to have high thermostability. However, native *Ld*MetAP1 showed higher thermostability (T_M 354.5 ± 0.3 K) than T291A (T_M 347.5 ± 0.3 K) possibly due to more helices (Fig. 3B).

2.3 *Ld*MetAP1 is a Fe(II) dependent methionine aminopeptidase

Methionine aminopeptidases are exopeptidases implicated in the excision of initiator methionine residue from nascent polypeptides. Therefore, amidolytic activity of *Ld*MetAP1 was assessed using a synthetic substrate L-methionine-4-methyl-coumaryl-7-amide in the presence of different metal chlorides. The kinetic parameters determined with different metals at the physiological pH (Supplementary Fig. 1A) revealed *Ld*MetAP1 to be highly activated by divalent cobalt (Fig. 3C). However, *Ld*MetAP1 showed highest affinity for fluorogenic substrate when it was supplemented with divalent iron (K_m = 40.4 ± 5.4 μM) in the assay buffer. This points towards the *Ld*MetAP1 being an iron-dependent aminopeptidase (k_{cat}/K_m = 114.71 ± 16.28 × 10^3 $M^{-1}min^{-1}$) than a cobalt-dependent aminopeptidase (k_{cat}/K_m = 67.62 ± 4.73 × 10^3 $M^{-1}min^{-1}$). The other major activators of *Ld*MetAP1 were divalent manganese (k_{cat}/K_m = 41.71 ± 3.85 × 10^3 $M^{-1}min^{-1}$) and magnesium (k_{cat}/K_m = 23.36 ± 2.92 × 10^3 $M^{-1}min^{-1}$), while zinc didn't prove to be a good activator for the amidolytic activity of *Ld*MetAP1 (Table 1).

While assessing whether *Ld*MetAP1 can cleave other residues from the synthetic substrates, we tested other fluorogenic substrates in *in vitro* aminopeptidase assay. Unlike *Ld*MetAP2, the enzyme *Ld*MetAP1 doesn't prefer the cleavage of smaller amino acid residues like Ala from Ala-AMC (Fig. 3D). In fact, *Ld*MetAP1 didn't cleave alanine at all. However, *Ld*MetAP1 hydrolyzed Leu from L-leucine-4-methyl-coumaryl-7-amide and showed minimal activity for di- and tripeptides. The results suggested *Ld*MetAP1 to be specific to methionine hydrolysis and highlighted the bigger residue preference of this enzyme for activity.

2.4 Identification of selective *Ld*MetAP1 Quinoline-carbaldehyde core bearing inhibitors

We synthesized 20 Quinoline-carbaldehyde derivatives (Fig. 1) and screened them in aminopeptidase assays. Synthesis of the target compound **4** was carried out in 2 steps as illustrated in Scheme-1. In the first step, the commercially available 8-Hydroxy-2-methylquinoline (**1**) was subjected to oxidation with SeO_2 to obtain the corresponding 8-hydroxy-2-quinoline carbaldehyde (**2**) by using the reported method [19]. Subsequently, 8-hydroxy-2-quinoline carbaldehyde (**2**) was subjected to cyclization reaction with substituted anilines and thioglycolic acid as per the literature report [20] to afford the final product [**4 (HQ1-HQ20)**]**.** The purity analysis by HPLC has demonstrated all compounds to be highly pure except HQ11 which possessed degradative tendency (Supplementary Table 1). The newly synthesised compounds were confirmed and characterized by spectroscopic techniques such as, ^{1}H-NMR and ^{13}C-NMR etc. The ^{1}H-NMR spectra demonstrated characteristic peaks around 3.8 ppm and 4.1 ppm region which corresponds to CH_2 of the 4-thiazolidinone ring. Whereas, the peak at 7.26 ppm as singlet corresponds to the CH attached to quinoline ring. In ^{13}C-NMR, peaks around 3.94 ppm and 65.53 ppm are those of 4-thiazolidinone carbons while, a peak at 171 ppm corresponds to the carbonyl carbon of the 4-thiazolidinone. The DEPT ^{13}C-NMR studies were performed for the three most active compounds HQ13, HQ14 & HQ15 to confirm the final products. DEPT spectra of compound 14 demonstrated a characteristic negative peak at 33.13 ppm which corresponds to CH_2 of 4-Thaizolidinone ring, whereas the positive peak at 66.35 is due to CH of 4-Thiazolidinone and peak at 20.97 is due to CH_3 of aromatic rings (Supplementary material). The remaining peaks are that of the aromatic ring. Four promising compounds showing encouraging inhibition of *Ld*MetAP1 were identified and their relative potency for the specific inhibition of *Ld*MetAP1 was determined by enumerating the IC_{50} values in inhibition assay (table 2). The most potent

inhibitors (HQ11, HQ13, HQ14 and HQ15) were then again tested for selectivity using both *Ld*MetAP1 and *Hs*MetAP1 enzymes. While as, HQ11 showed a similar potency for *Ld*MetAP1 and *Hs*MetAP1 enzymes, inhibitors HQ13, HQ14 and HQ15 were highly specific to *Ld*MetAP1 (Fig. 4A-D and Supplementary Fig. 3A). Using time course assays of 30 min, we determined the mode of inhibition of promising inhibitors of *Ld*MetAP1. HQ11 which inhibits *Ld*MetAP1 (IC_{50} 8.8 μM) and *Hs*MetAP1 (IC_{50} 8.9 μM) with almost equal potency was found to inhibit *Ld*MetAP1 in an uncompetitive manner as both K_m and V_{max} decreased with soaring HQ11 (Fig. 4E). Other hit compounds (HQ13, HQ14 and HQ15) inhibited *Ld*MetAP1 through a competitive mode of inhibition as K_m showed an increase and V_{max} stood steady with an increase in the concentration of these inhibitors (Fig. 4F-H). A substitution at the C4 position of the six carbon ring appeared to be essential for potency as other substitutions didn't seem to contribute greatly to the inhibitor potency. Interestingly, barring a –CN group substitution at C3, other substitutions made at this position didn't seem to add to inhibitor potency. In contrast, all substitutions made at C4 contributed to potency. Hence, different analogs bearing different groups at C4 position were synthesized (Fig. 1). Positioning of a chloride atom at C4 position as in HQ15 increased the inhibitor potency greatly rendering HQ15 as the most potent inhibitor (IC_{50} 1.1 μM) of *Ld*MetAP1 in this library (Fig. 4D). Substitution of smaller electronegative atom amongst halogens like fluorine (IC_{50} 45.4 μM) or a bigger atom of the same group like bromine (IC_{50} 251.6 μM) at C4 position was found inefficient in inhibition assays (Supplementary Fig. 1B). Addition of a -CH_3 group as in HQ14 (IC_{50} 1.3 μM) showed good potency as well (Fig. 4C).

We next determined the toxicity of hit compounds with MTT assay and found all compounds except HQ11 exhibiting low toxicity. While determining whether the identified hits have druglikeness, we determined physiochemical properties along with the parameters like LogP,

LogS and GI absorption. We found all hits possess promising druglikeness as none of them violated the Lipinski's rule (Table 3).

2.5 Lead molecules HQ11, HQ13, HQ14 and HQ15 bind to *Ld*MetAP1 with high affinity

Physical interactions of enzymes *Ld*MetAP1 and *Hs*MetAP1 with HQ11, HQ13, HQ14 and HQ15were monitored using Surface plasmon resonance (SPR) binding assays. Sensorgrams showed a direct interaction between HQ compounds and recombinant enzymes with HQ11 binding (Fig. 5A and B) with high affinity to both *Ld*MetAP1 (K_D 1.61 × 10^{-10}M) and *Hs*MetAP1 (K_D 1.52 × 10^{-10} M). Other leads HQ13, HQ14 and HQ15 had higher binding affinities (Table 4) for *Ld*MetAP1 (Fig. 5C, E and G) than *Hs*MetAP1 (Fig. 5D, F and H). Indeed, lead inhibitor molecule HQ15 showed comparatively lesser affinity for *Hs*MetAP1 (K_D 3.61 × 10^{-7} M) and higher affinity for *Ld*MetAP1 (K_D 1.50 × 10^{-8} M) which explains its poor inhibition of *Hs*MetAP1. Meanwhile, fluorescence spectroscopic plots showed all lead molecules HQ11, HQ13, HQ14 and HQ15 quenching the fluorescence emission of *Ld*MetAP1 in a concentration dependent manner (Supplementary Fig. 2A-D). Determination of the binding parameters using modified Stern-Volmer plots showed all lead molecules to have high binding affinity for *Ld*MetAP1 which corroborates with the surface plasmon resonance results.

2.6 Quinoline-carbaldehyde specificity and potency is majorly mediated through a Thr residue unique to *Ld*MetAP1

Quinoline-carbaldehyde core bearing compound library showed specificity to *Ld*MetAP1 and not to *Hs*MetAP1 even though *Ld*MetAP1 and *Hs*MetAP1 have high structural similarity and an identical domain and fold organization. However, amino acid sequences of *Ld*MetAP1 and *Hs*MetAP1 carry key amino acid differences at S1 and S1' sub-sites (Fig. 2D). Molecular

docking of hit compounds with *Ld*MetAP1 suggests Thr291, His300 and Asn304 to be the key residues involved in inhibitor binding. Since His300 and Asn304 are conserved in both *Ld*MetAP1 and *Hs*MetAP1 enzymes, we reasoned they may not be the key residues conferring inhibitory specificity. However, Thr291 is unique to *Ld*MetAP1, and is replaced by Cys in *Hs*MetAP1. Mutation of Thr291 with either Ala or Val resulted in the loss of affinity of specific inhibitor HQ15 to *Ld*MetAP1 from -7.4 kcal/mol to -6.8 kcal/mol in computational assays (Fig. 6E-G). We followed up computational assays by site directed mutagenesis and mutated Thr291 to Ala. While determining whether there was a change in the catalytic efficiency of *Ld*MetAP1 after mutating Thr291 to Ala, we performed aminopeptidase assay of mutazyme T291A and found it catalytically less efficient (Fig. 6A). Moreover, there was a remarkable loss in affinity of T291A for substrate (K_m 969.7 ± 215.1µM), indicating Thr291 to be an important substrate binding residue for *Ld*MetAP1. Intriguingly, inhibition assays of *Ld*MetAP1 and T291A with inhibitors HQ13, HQ14 and HQ15 suggested T291A to be very less prone to inhibition by specific inhibitors than the native *Ld*MetAP1 (Fig. 6B-D and Supplementary Fig. 3B). This demonstrated Thr291 to be a crucial specificity conferring residue for the inhibition of *Ld*MetAP1 by Quinoline-carbaldehyde core bearing competitive inhibitors.

2.7 Structural basis of inhibition of *Ld*MetAP1

In an attempt to unravel the atomic interactions of lead compounds with *Ld*MetAP1, we performed molecular docking studies. For analysis the conformation of ligands with protein having the highest binding affinity was chosen. Firstly, the ligand binding site of HQ11 (uncompetitive inhibitor of *Ld*MetAP1) was predicted. HQ11 was found interacting with *Ld*MetAP1 exclusively via hydrophobic interactions involving residues Arg107, Gly108, Asp106, Pro240, Thr291, Gly292, His293, Thr301, Ala302 and Asn304 (Fig. 7A). HQ13 had

a lone hydrogen bond with Thr291 and hydrophobic interactions with residues Tyr185, Tyr290, Gly292, His293, His300, Glu326 and Trp343 (Fig. 7B). Furthermore, both HQ14 and HQ15 interact with Thr291, His300 and Asn304 through hydrogen bonding and have hydrophobic interactions with residues Arg107, Tyr185, Tyr186, Ser289 and Tyr290 (Fig 7C and D). Therefore, lead molecules HQ14 and HQ15 bind *Ld*MetAP1 via three hydrogen bonds while as, HQ13 and HQ11 bind to *Ld*MetAP1 via one and no hydrogen bonds, respectively. The binding site and binding mode of HQ11 was contrastingly different from those of HQ13, HQ14 and HQ15 which bind at the catalytic active site providing a structural basis for the differences in the mode of inhibition. Meanwhile, all leads bound *Hs*MetAP1 with different binding modes and lower affinity (except HQ11) which may be a major contributing factor to the exceptionally lower potency of HQ13, HQ14 and HQ15 against *Hs*MetAP1 (Fig. 7E-H).

2.8 Lead inhibitor HQ15 forms a stable complex with *Ld*MetAP1

After molecular docking of all lead compounds, *Ld*MetAP1 and T291A were simulated alone and in complex with lead molecule HQ15 for 30 ns. RMSD of backbone atoms used to assess the convergence of structure to equilibrium after HQ15 binding suggested *Ld*MetAP1 and T291A to be stable as there was no significant deviation in the RMSD. The binding of HQ-15 to both *Ld*MetAP1 as well as T291A increased the RMSD by approximately 0.8 Å (0.08 nm) suggesting a minor change induced in the protein structure after ligand binding (Fig. 8A). This matches with the fluorescence spectroscopic studies where HQ15 binding quenched the fluorescence but didn't affect the protein folding greatly as neither a 'blue shift' nor 'red shift' was observed (Supplementary Fig. 2D). Meanwhile, both *Ld*MetAP1-HQ15 as well as T291A-HQ15 complex reached equilibrium one after another with former assuming precedence.

The flexibility of unbound and HQ15 bound enzymes during the 30 ns MDS run was assessed by plotting RMSF. Other than the major fluctuations occurring in the C-terminal region (residues 310-315) and with non-catalytic residues Cys221 and Ser250 (of truncated *Ld*MetAP1) which are far off from the catalytic pocket, all systems were highly rigid (Fig. 8B). Specific fluctuations in the loop region towards C-terminal end possibly indicate the occurrence of slight conformational changes after HQ15 binding.

Unbound and HQ15 bound enzyme structures were also analyzed using Rg which describes compactness by measuring the mass of atoms relative to the mass of whole complex. *Ld*MetAP1 showed relatively more compactness than T291A. Furthermore, *Ld*MetAP1-HQ15 complex had higher compactness than T291A-HQ15 complex. Therefore, the compactness and stability of *Ld*MetAP1 increased dramatically after complex formation with HQ-15 (Fig. 8C). The MD simulations of *Ld*MetAP1 and T291A and its complexes with HQ15 assert the complexes to be stabilized by conformational rearrangements and that HQ15 like other lead molecules is held with *Ld*MetAP1 by hydrophobic interactions and hydrogen bonding. Similar results were observed through molecular docking.

3. Discussion

The removal of initiator methionine from nascent polypeptides by MetAPs is an evolutionary conserved process essential for growth, proliferation and survival of both prokaryotes and eukaryotes. Like human and yeast genome, the leishmanial genome encodes both type I and type II forms of MetAPs. Deletion of MetAPs from the yeast or other eukaryotic genomes causes growth and developmental abnormalities and leads to lethality [16,21]. Moreover, specific inhibition of MetAPs with small molecule inhibitors leads to immune suppression [22] and blockade of angiogenesis in humans [23]. Specific and potent inhibition of MetAPs has also been used to evade and eliminate parasitic infections [24] suggesting specific

inhibition or inactivation of leishmanial MetAPs could become a mainstream strategy to block the growth and proliferation of *L. donovani*. We cloned, expressed and purified both *Ld*MetAP1 and *Hs*MetAP1 and established that both of these recombinantly expressed enzymes are active under physiological like conditions against a synthetic fluorogenic substrate L-methionine-4-methyl-coumaryl-7-amide widely used to determine activity of MetAPs and inhibitor screening.*Ld*MetAP1 showed high catalytic efficiency than *Hs*MetAP1 [25] and *Tb*MetAP1 [26] at physiological pH. While screening other synthetic substrates carrying a smaller or bigger P^1 residue (such as, Ala or Leu), we found *Ld*MetAP1 either inactive or marginally active suggesting its high specificity for the hydrolysis of Met. Like other type I MetAPs, *Ld*MetAP1 was highly activated by divalent cobalt which can be attributed to the ability of this metal to act as a hard Lewis acid [27] as a result of which it attains high affinity for hard bases like water or hydroxide ions that are involved in the catalytic mechanism [28] of MetAPs. Furthermore, cobalt has a partially filled 3d orbital and thence preferred oxidation states of +2 and +3 which allow it to form low-spin trigonal bipyramidal, high-spin octahedral and low-spin octahedral complexes [26]. Because of the higher stability of cobalt's low-spin and high coordination number complexes, the metal ion charge intensifies which leads to higher substrate binding and the stability of reaction intermediates. Such chemical properties result in higher catalytic efficiency of cobalt activated MetAPs. Although highly activated by Co(II), *Ld*MetAP1 had highest affinity for substrate when activated by Fe(II) much like *Ec*MetAP1 [13]. In fact, *Ld*MetAP1 seemed specific to Fe(II) as the substrate binding increased dramatically. Interestingly, the concentration of cytosolic Fe(II) increases while the concentration of Co(II) stays steady when *Ec*MetAP1 is over-expressed in *E. coli* which further supports the narrative that iron is the physiological activator of type I MetAPs. Like *Tb*MetAP1 [26], *Ld*MetAP1 didn't show a noticeable activity with Zn(II) against L-methionine-4-methyl-coumaryl-7-amide. Whether or

not *Ld*MetAP1 can be activated by Zn(II) like *Tb*MetAP1 [26] against other substrates that resemble physiological substrates of MetAPs like Met-Gly-Met-Met remains to be seen. Zinc is the second most plenteous metal in human body [29] and is resistant to redox changes at biological potential [30]. Therefore, it is difficult to rule out the possibility of zinc being one of the major physiological activators of MetAPs. Structurally, MetAPs are very similar; therefore, different metal preferences can be due to amino acid substitutions near the catalytic site allowing slight rearrangement of active site residues which alter metal preferences and metal dependence. As such, *Hs*MetAP1 could be highly activated by Co(II) due to a smaller active site [31]. All type 1 MetAPs including *Ld*MetAP1 are monomeric in solution and have a two domain organization i) N-terminal domain which reportedly binds to ribosome [32] to take up the N-terminal methionine processing of nascent polypeptides and ii) C-terminal catalytic domain which carries catalytic residues DDHEE embedded with two divalent metal ions indispensable for catalysis [7,28]. Modelled *Ld*MetAP1, like the crystal structure of *Tb*MetAP1 carries more β-sheets than α-helices. This in turn matches with the Far-UV CD spectroscopic data whose analysis suggested that *Ld*MetAP1 carries 21% α-helices and 24% β-sheets.

While screening inhibitor libraries of distinct structural classes, we identified quinoline-carbaldehyde core bearing inhibitors HQ14 and HQ15 which inhibited *Ld*MetAP1 specifically. Most inhibitors of this library except HQ11 showed remarkably high specificity towards *Ld*MetAP1 than *Hs*MetAP1 possibly due to crucial amino acid substitutions near the catalytic site. The key structural element necessary for inhibitors to carry potency was the C4 position of the 6-carbon ring linked to the quinoline-carbaldehyde core by a Nitrogen atom of pentameric ring. Multiple substitutions with different groups revealed –Cl substitution to be most efficient for potency while $–CH_3$ substitution was equally efficient. Thr291 of *Ld*MetAP1 appeared to be directly interacting with leads and crucial to mediate inhibitor

potency as mutazyme (T291A) carrying Ala at the place of Thr was less susceptible to inhibition by competitive inhibitors HQ13, HQ14 and HQ15. Thr291 is an important substrate binding residue whose mutation to Ala or Val caused rotameric flipping of active site residues and the residues surrounding active site like Arg107, Tyr185, Tyr290, His293 and Asn304 which potentially alters inhibitor potency. Interestingly, Thr is replaced by Cys in *Hs*MetAP1 and is not prone to inhibition by HQ13, HQ14 and HQ15. Meanwhile, T291A was comparatively less thermostable than *Ld*MetAP1 possibly due to a slight decline in the percentage of α-helices. Decline in α-helices tends to destabilize protein structures and renders them vulnerable to denaturation [33]. Furthermore, time course biochemical experiments suggested inhibitor HQ11 which carries a fluorine substitution at the C3 position of the 6-carbon ring linked to the quinoline-carbaldehyde core binding *Ld*MetAP1 at a site other than the active site. Similar observations were made with molecular docking. This could be due to the highly electronegative nature of fluorine [34] that enables the inhibitor (HQ13) to either bind at multiple sites to the enzyme or bind away from the active site rich in highly reactive residues as depicted by molecular docking studies. Interestingly, HQ11 was equally potent against *Ld*MetAP1 and *Hs*MetAP1 with similar binding affinities implying it could have a common binding site in both enzymes. This is indeed possible as *Ld*MetAP1 and *Hs*MetAP1 carry a high sequence homology in the C-terminal catalytic domain and have almost identical structures. In contrast, inhibitors HQ13, HQ14 and HQ15 seemed specific to *Ld*MetAP1 and inhibited it competitively with similar binding modes and encouraging IC_{50} values. Surface plasmon resonance and fluorescence spectroscopic measurements suggested all lead inhibitors binding *Ld*MetAP1 with higher affinity than *Hs*MetAP1 except HQ11 which binds to both enzymes with high affinity. HQ11 also carries toxicity possibly because of off-target binding due to the presence of reactive fluorine in the hexameric ring. Other lead molecules specific to *Ld*MetAP1 *viz* HQ13, HQ14 and HQ15 showed comparatively low

toxicity and drug likeness. Importantly, lead molecule HQ15 also formed a stable complex with *Ld*MetAP1 in a 30 ns MDS run suggesting this to be an important lead for inhibitor development against *Ld*MetAP1. The molecular basis of remarkably high potency and specificity of HQ14 and HQ15 towards *Ld*MetAP1 and not *Hs*MetAP1 remains largely unknown. However, specificity may manifest due to crucial amino acid differences between *Ld*MetAP1 and *Hs*MetAP1 within 6 Å distance from the catalytic site. The differing residues: (*Ld*MetAP1 vs. *Hs*MetAP1) Val220 vs. Ile221, Ser221 vs. Thr222, Thr291 vs. Cys292 render *Hs*MetAP1 catalytic site compact due to bulkier side chains which possibly makes it inaccessible to quinoline-carbaldehyde core containing leads and thus, less vulnerable to inhibition.

Specific inhibitors of *Ld*MetAP1 have a potential to circumvent the mayhem of drug resistance to current regimen of antileishmanials which has also been a major roadblock for the effective elimination of leishmaniasis. Identification of specific *Ld*MetAP1 inhibitors have a potential to aid the development of new antileishmanial agents. Moreover, specific inhibitors of *Ld*MetAP1 like HQ14 and HQ15 may also be used to inhibit the growth and proliferation of both promastigotes and amastigotes as *Ld*MetAP1 is a vital house-keeping enzyme expressed in both life forms of *Leishmania* species thereby extending the importance and efficacy of specific *Ld*MetAP1 inhibitors. Improvement to lead molecules like HQ14 and HQ15 along with other quinoline-carbaldehyde core bearing inhibitors in their selectivity and potency toward *Ld*MetAP1 over *Hs*MetAP1 may thus lead to the development of a novel class of antileishmanial agents.

4. Experiments

4.1 Sequence analysis and Homology modelling

*Ld*MetAP1 sequence was identified through HMMER web server (https://www.ebi.ac.uk/Tools/hmmer/) which also described this enzyme to be a member of M24 aminopeptidases. The sequence was further analysed with web based SMART server [35] for motif analysis, domain organization and presence of signal peptide and internal repeats. For physico-chemical properties ProtParam tool was used (https://web.expasy.org/protparam/). Homology model of *Ld*MetAP1 was generated with the program Modeller 9.15 version [36] using the structural coordinates of *T. brucei* methionine aminopeptidase 1 (PDB code: 4FUK) as a template (sequence identity, 70%). The loops and Ramachandran outliers were fixed and the modelled structure was energy minimized with Gromacs 4.6.3 [37]. The geometry of model was validated with RAMPAGE [38] and the structure was visualized in PyMOL [39].

4.2 Cloning and site directed mutagenesis

Gene sequence encoding for functional *Ld*MetAP1 was amplified from the genomic DNA of *Leishmania donovani* DD8 strain using primers specific for *Ld*MetAP1 (5'-ATTGGATCCATGGTGGACGAGCGGCTCTTCAAC-3' and 5'-AGCAAGCTTTCAGATTTTGATTTCGCTGGGGTC-3'). Likewise, ORF of *Hs*MetAP1 containing 1161 nucleotides was amplified from the cDNA (generated from the mRNA isolated from human fibroblasts) using primers (5'-TTAGGATCCATGGCGGCCGTGGAGACG-3'and 5'-AGGCTCGAGTTAAAATTGAGACATGAAGTGAG-3'). The PCR products of both genes were cloned in the expression vector pET28a in frame with an N-terminal 6x-Histidine tag between the sites *Bam*HI and *Hind*III, and *Bam*HI and *Xho*I, respectively. Both clones were

confirmed by restriction digestion and DNA sequencing. Meanwhile, Thr291 positioned at the active site of *Ld*MetAP1 structure was mutated to Ala in a PCR reaction using primers containing a mutation (5'-GATACCATGCCCGGCGTAGCTGCGCACTA-3' and 5'-TAGTGCGCAGCTACGCCGGGCATGGTATC-3'). The PCR was performed as follows: 98 ℃ for 30 sec, 98 ℃ for 30 sec, 60 ℃ for 1 min, 72 ℃ for 6 min 30 sec and 72 ℃ for 10 minutes. Methylated template plasmid DNA was digested with *Dpn*I for 1 hr at 37 ℃ and the reaction was transformed into XL1-Blue cells. The transformants observed on plate were grown in LB media for plasmid extraction to confirm the mutation with DNA sequencing.

4.3 Expression and purification of recombinant enzymes

For *Ld*MetAP1, T291A and *Hs*MetAP1 expression, *E. coli* BL21 (DE3) cells were used and the protein expression induced with 0.5 mM IPTG for 20 hours at 18°C in a shaking incubator. The IPTG induced *E. coli* BL21 (DE3) cultures expressing *Ld*MetAP1, T291Aand *Hs*MetAP1 were harvested by centrifugation at 4°C and resuspended in the lysis buffer (50 mM Tris-HCl pH 8.0, 250 mM NaCl and 25mM imidazole). Cells were lysed by sonication and the cell lysate centrifuged at 14000 rpm at 4°C for 45 minutes. The resultant supernatant was loaded onto a pre-packed His-Trap column (GE Healthcare) equilibrated with the lysis buffer for protein binding on an AKTA purification system (GE Healthcare). After extensive washes, all enzymes were eluted out with a buffer bearing 50 mM Tris-HCl (pH 8.0), 250 mM NaCl & 250 mM imidazole. The protein size and quality was checked on 10% (w/v) SDS-PAGE. The purest fractions of *Ld*MetAP1 were concentrated and loaded onto a pre-calibrated Superdex 200 column (GE Healthcare) for size-exclusion chromatography. The protein concentration was estimated photometrically on Nano drop (Thermo Scientific) using molar absorption coefficient and molecular weight of 45380 mol^{-1} cm^{-1} and 41480 Da for *Ld*MetAP1 and 55350 mol^{-1} $cm^{-1}$and 46252Da for *Hs*MetAP1, respectively.

4.4 Circular Dichroism (CD) measurements

Far-UV CD spectra of *Ld*MetAP1 and T291A (3 μM each in 10 mM Potassium phosphate buffer, pH 7.2) were recorded in a quartz cell of 0.2 cm path length on JASCO-J1500 CD spectropolarimeter. For thermo-stability assays, spectral changes of *Ld*MetAP1 and T291A were analyzed in the temperature range of 293 to 380 K and the data fitted into the two-state equilibrium unfolding model to enumerate thermodynamic parameters in Sigma plot 12.0 (San Jose, USA). CD spectral data was analyzed with the program DICHROWEB to predict secondary structures of *Ld*MetAP1 and T291A.

4.5 Aminopeptidase activity assay

The *Ld*MetAP1, T291A and *Hs*MetAP1 activity was estimated by measuring the excision of L-methionine from fluorogenic substrate L-methionine-4-methyl-coumaryl-7-amide (Sigma Aldrich, USA) using InfiniteM200 Pro spectrofluorometer (TECAN, Switzerland) with a wavelength pair of 355 and 460 nm used for excitation and emission, respectively. The aminopeptidase activity assay buffer was supplemented with a metal chloride and 0.5 μM *Ld*MetAP1. After incubation at 37°C for 30 minutes, the substrate was added up to a final concentration of 200 μM and the activity recorded in a 30 minute kinetic cycle with a break of 1 min between measurements. To test whether *Ld*MetAP1 cleaved other amino acid residues, fluorogenic substrates L-alanine--4-methyl-coumaryl-7-amide, L-leucine-4-methyl-coumaryl-7-amide, L-arginine-4-methyl-coumaryl-7-amide, L-lysine-alanine-4-methyl-coumaryl-7-amide, L-alanine-alanine-phenylalanine-4-methyl-coumaryl-7-amide, L-alanine-leucine-lysine-4-methyl-coumaryl-7-amide and L-alanine-alanine-phenylalanine-4-methyl-coumaryl-7-amide were tested in aminopeptidase assays. Fluorescence emission due to peptide bond hydrolysis was converted into product formation (AMC) and the steady state kinetic parameters determined in Graphpad Prism.

4.6 Chemistry

General procedure for the Synthesis of compound 2: (8-Hydroxxy-2-quinolinecarbaldehyde)

8-hydroxy-2-methylquinoline (**1**) (2g, 12.4 mmol.), selenium dioxide (1.74g, 15.8 mmol), 300 ml of degassed 1, 4-dioxane, and 1.5 ml of water were mixed and stirred in a 1L round bottom flask. The resulting solution was then refluxed for 24 hours and the reaction was monitored until completion using TLC method. The reaction mixture was then filtered off, and the selenium metal was washed with dichloromethane, and the combined filtrates were then evaporated off under reduced pressure. The crude product was purified by sublimation under reduced pressure or by silica gel column chromatography to yield pure yellow needle crystal. Yellow solid; Yield = 74.5%; Melting point = 97.0-98℃; **^{1}H NMR (500 MHz, $CDCl_3$)** δ 10.22 (s, 1H), 8.32 (d, J = 8.5 Hz, 1H), 8.17 (s, 1H), 8.06 (d, J = 8.5 Hz, 1H), 7.63 (t, J = 8.0 Hz, 1H), 7.44 (dd, J = 8.3, 0.8 Hz, 1H), 7.29 (dd, J = 7.8, 1.0 Hz, 1H). **^{13}C NMR (125 MHz, $CDCl_3$)** δ 192.72 (s), 153.02 (s), 150.17 (s), 137.81 (s), 137.49 (s), 130.96 (s), 130.44 (s), 118.04 (d, J = 11.5 Hz), 111.26 (s).

General procedure for one pot synthesis of 8-Hydroxyquinoline-substituted 4-Thiazolidinones [4 (HQ1-HQ20)]

To a solution of substituted anilines (0.867 mmol, 1eq) in Dichloromethane at 0°C, 8-Hydroxy-2-Quinolinecarbaldehyde (**2**) (1.300 mmol, 1.5eq) was added and the mixture stirred for 5 min. Thioglycolic acid (1.734 mmol, 2eq) was then added to the above reaction and stirring was continued for another 5 min at 0°C followed by the addition of silica gel (0.5 g, 100-200 mesh) as shown in Scheme 1. The reaction was stirred for 4 hr at room temperature and the reaction progress monitored by TLC. After completion of the reactions as indicated by TLC, the reaction mixture was extracted with DCM and the extract was washed with sodium bicarbonate solution. The DCM layer was collected and concentrated to

give the crude product which was purified by using silica gel (100-200) column chromatography by using 5% ethylacetate-hexane as eluent to get the pure product [**4 (HQ1-HQ20)**] with 60-75% yield (Table 5).

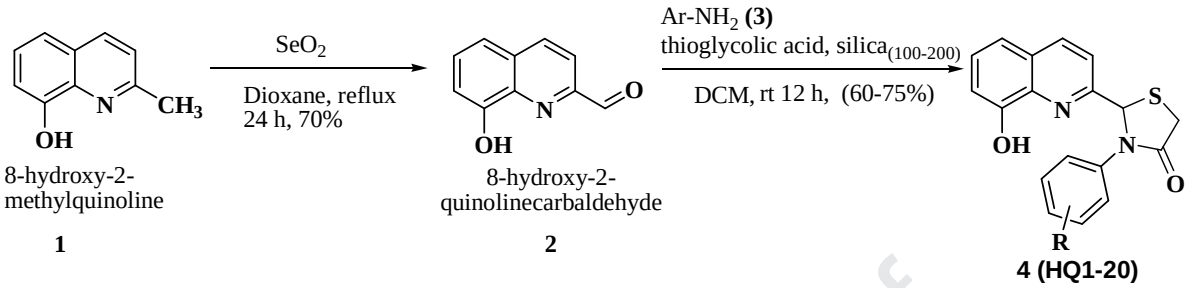

Scheme 1: General synthesis scheme of new target molecules (**4**)

For purity analysis, all HQ molecules were subjected to HPLC by employing Isocratic method and Phenomenex C8 150 X 4.6 column on Waters e2695 module with quaternary solvent manager system using mobile phase [0.1 % Formic acid and Acetonitrile (30:70)] for a run time of 10 min at 25°C. All the compounds were characterised by spectroscopic methods and the spectral data is given in supplementary material. Spectral data for the selected compounds HQ13, HQ14 and HQ15 are given below:

HQ13 (3-(2-(8-hydroxyquinolin-2-yl)-4-oxothiazolidin-3-yl)benzonitrile): Yield;70% , white solid, MP;175-178°C; IR(ATR); 3416.79, 2971.13, 2889.70, 2233.18, 1681.40, 1601.18, 1393.28, 1046.46 cm^{-1}; ^{1}H NMR (500 MHz, $CDCl_3$) δ 8.21 (d, J = 8.5 Hz, 1H), 7.75 (d, J = 6.9 Hz, 2H), 7.57 (ddd, J = 8.1, 2.1, 1.3 Hz, 1H), 7.40 (dddd, J = 18.8, 12.1, 9.0, 4.4 Hz, 5H), 7.21 (dd, J = 7.6, 0.9 Hz, 1H), 6.34 (s, 1H), 4.06 (dd, J = 16.0, 1.1 Hz, 1H), 3.87 (d, J = 16.0 Hz, 1H); ^{13}C NMR (125 MHz, $CDCl_3$) δ 171.38 (s), 156.06 (s), 151.92 (s), 138.66 (d, J = 9.0 Hz), 137.13 (s), 130.06 (d, J = 11.0 Hz), 128.72 (s), 128.06 (s), 127.32 (s), 118.43 (s), 117.95 (d, J = 14.9 Hz), 113.40 (s), 111.42 (s), 65.53 (s), 32.94 (s); HRMS; m/z calculated for $C_{19}H_{13}N_3O_2S$ [M+H]+ :348.0807; found : 348.0804.; ^{13}C NMR (DEPT) (126 MHz, $CDCl_3$) δ 138.68 (s), 130.06 (d, J = 10.8 Hz), 128.71 (s), 128.08 (s), 127.34 (s), 118.45 (s), 118.01 (s), 111.42 (s), 65.54 (s), 32.94 (s).

HQ14 (2-(8-hydroxyquinolin-2-yl)-3-(p-tolyl)thiazolidin-4-one): Yield; 72%, white solid, MP;123-125°C; IR(ATR); 3422.63, 2917.71, 1683.64, 1502.03, 1329.42 cm^{-1}; ^{1}H NMR (500 MHz, $CDCl_3$) δ 8.16 (d, *J* = 8.6 Hz, 1H), 7.91 (s, 1H), 7.49 (s, 1H), 7.47 (d, *J* = 4.8 Hz, 1H), 7.44 (d, *J* = 8.0 Hz, 1H), 7.31 (t, J = 8.6 Hz, 1H), 7.26 (s, 1H), 7.18 (d, *J* = 8.4 Hz, 3H), 7.07 (d, *J* = 8.3 Hz, 2H), 6.33 (s, 1H), 4.06 (dd, *J* = 15.8, 1.5 Hz, 1H), 3.88 (d, *J* = 15.8 Hz, 1H), 2.23 (s, 3H); ^{13}C NMR (125 MHz, $CDCl_3$) δ 171.21 (s), 157.22 (s), 151.92 (s), 138.33 (s), 137.18 (s), 134.81 (s), 129.93 (s), 128.44 (s), 128.01 (s), 124.90 (s), 118.80 (s), 117.88 (s), 111.23 (s), 66.16 (s), 33.13 (s), 20.97 (s); HRMS; m/z calculated for $C_{19}H_{16}N_2O_2S$ $[M+H]^+$:337.1011; found : 337.1014.

HQ15 (2-(8-hydroxyquinolin-2-yl)-3-(4-chlorophenyl)thiazolidin-4-one): Yield; 80%, pale yellow crystals, MP;133-135°C; IR(ATR); 3470.07, 3203.07, 2900.07, 1689.91, 1596.44, 1490.38, 1328.08, 769.62 cm^{-1}; ^{1}H NMR (500 MHz, $CDCl_3$) δ 8.17 (d, J = 8.6 Hz, 1H), 7.84 (s, 1H), 7.46 (dd, J = 17.7, 8.2 Hz, 2H), 7.33 – 7.26 (m, 3H), 7.25 – 7.18 (m, 3H), 6.32 (s, 1H), 4.05 (dd, J = 15.9, 1.3 Hz, 1H), 3.87 (d, J = 15.9 Hz, 1H); ^{13}C NMR (125 MHz, $CDCl_3$)) δ 171.22 (s), 156.65 (s), 151.92 (s), 138.46 (s), 136.99 (s), 136.08 (s), 132.52 (s), 129.40 (s), 128.59 (s), 128.02 (s), 125.81 (s), 118.62 (s), 117.94 (s), 111.32 (s), 65.91 (s), 33.05 (s); HRMS; m/z calculated for $C_{18}H_{13}ClN_2O_2S$ [M+H]+ :357.0465; found : 357.0463.; ^{13}C NMR (DEPT) (126 MHz, $CDCl_3$) δ 138.35 (s), 129.39 (s), 128.54 (s), 125.83 (s), 118.66 (s), 117.95 (s), 111.20 (s), 66.00 (s), 33.06 (s).

4.7 *Ld*MetAP1 *in vitro* inhibition assay

Twenty Quinoline-carbaldehyde derivatives (Fig. 1), dissolved in 100% DMSO, were screened as inhibitors for *Ld*MetAP1 and *Hs*MetAP1 (as control) in 96-well plates to identify hits. Initially, the enzyme present in the assay buffer along with the metal supplement was incubated for 30 minutes. Post-incubation, substrate L-methionine-4-methyl-coumaryl-7-

amide (125 μM) was added and the fluorescence recorded with InfiniteM200 Pro spectrofluorometer (TECAN, Switzerland). The net percentage decrease in fluorescence in comparison to the control enzymatic reactions was taken as percentage inhibition for every compound tested. The IC_{50} obtained for each compound with different concentrations was then used to identify and rank hits in the order of potency. For mode of inhibition, hit compounds were incubated with enzyme (0.5 μM) in Fe (II) supplemented assay buffer for 30 minutes at 37 °C. Subsequently, the substrate was added from 0-200 μM and the activity measurements recorded in a time course reaction for 30 minutes. The mode of inhibition was determined by Lineweaver-Burk plots.

4.8 Cell viability assay and assessment of druglikeness

For cell viability using MTT (3-(4,5-dimethylthiazol-2-yl)-2,5-diphenyltetrazolium bromide) assay, mouse embryonic fibroblast cells were incubated in media containing 0, 50, 100 and 200 μM concentration of compounds HQ11, HQ13, HQ14 and HQ15 for 48 h in 96-well plates. This was followed by the addition of MTT solution (5mg/ml) to each well and an incubation of 4 h at 37°C. Post incubation, the formazan crystals developed were dissolved by adding DMSO and gentle shaking at 37°C. Cell viability was determined spectrophotometrically by absorbance measurements at λ 570 nm. Furthermore, program SwissADME [40] was used for assessing physicochemical properties and druglikeness of all leads.

4.9 Surface Plasmon Resonance (SPR) binding assays and Fluorescence Spectroscopy

Enzymes (ligands) *Ld*MetAP1 and *Hs*MetAP1 were coupled to CM-5 dextran chip (GE Healthcare) with amine coupling. Binding assays were performed using common running and injection buffers composed of 1X PBS (pH 7.4) and 0.05% P-20. Analytes (HQ compounds)

dissolved in 2% DMSO were then passed over the immobilized enzymes to measure response units (RU) as a function of concentration of analytes. After solvent correction, kinetic analysis was carried out following a 1:1 Langmuir binding model in Biacore T200 evaluation software 2.0.

For Fluorescence measurements, 1 μM final concentration of *Ld*MetAP1 was taken in the buffer containing 20 mM Tris-HCl (pH: 7.5) and 50 mM NaCl at 25°C. Using five tryptophan residues of *Ld*MetAP1 as intrinsic fluorescent probes, the conformational changes of *Ld*MetAP1 with hit compounds were recorded (λ_{EX} ~ 295 nm, λ_{EM}~ 300-400 nm) using the Jasco ETC J-815 fluorescence spectrophotometer (Tokyo, Japan). After gentle mixing, *Ld*MetAP1 was incubated with hit compounds for 30 min at 25°C prior to fluorescence measurements. The relative fluorescence intensity obtained by (F_0/F_1), where F_0 and F_1 are the fluorescence intensities in the absence and presence of hits, was plotted against the hit concentration and the Stern-Volmer quenching constant (K_{SV}) calculated by linear regression in Graphpad Prism. Binding parameters of all compounds were calculated with modified Stern-Volmer plot as reported previously [41].

4.10 Molecular docking and Molecular Dynamics Simulations

For molecular docking with AutoDock Vina 1.1.2 [42] version using Lamarckian genetic algorithm, inhibitor coordinates were drawn manually and energy minimized. Docking studies were conducted following a grid based procedure as reported previously [7] with modifications in parameters and wherever necessary.

Molecular dynamics simulations consider receptor flexibility; therefore, this powerful method was used to assess the stability and rigidity of *Ld*MetAP1 and T291A separately and in complex with HQ15 using group parameters root mean square deviation (RMSD), root mean square fluctuation (RMSF), radius of gyration (Rg) and free energy calculations with

MM/PBSA method. The 30 ns production run was performed with Gromacs 4.6.3 [35] using GROMOS 96 43a1 as a force field. For complexes, HQ15 topology was built with PRODRG server [43] and the docking conformation with highest affinity was taken. Before production run, the topology of HQ15 was merged with both *Ld*MetAP1 and T291A separately and the simulations conducted following SPC model in a cubic box with water as a solvent. All other procedures used for 30 ns production run were adapted from our previous study [7].

Author Contributions

SYB performed the experiments, analyzed the data, and drafted the manuscript. PJ and AS synthesized the compounds used in this study under the guidance of MA. IAQ conceived, designed and supervised the study and revised the manuscript.

Acknowledgements

The authors are grateful to Council of Scientific and Industrial Research, India [CSIR, project no. 37(1686)/17/EMR-II], Government of India for funding. The authors acknowledge the instruments facilities supported by DST-FIST and UGC-SAP to the Department of Biotechnology & Bioinformatics, and Bioinformatics Infrastructure Facility, School of Life Sciences, University of Hyderabad, Hyderabad for computational resources. SYB thanks to Indian Council of Medical Research (ICMR) for Senior Research Fellowship. The authors gratefully acknowledge Prof. Swati Saha for providing genomic DNA of *Leishmania donovani* for this work.

Conflict of interest

The authors declare to have no conflict of interest whatsoever.

References

[1] S. Burza, S.L. Croft, M. Boelaert, Leishmaniasis, The Lancet. 392 (2018) 951-970, doi:10.1016/S0140-6736(18)31204-2.

[2] S. Sundar, J. Chakravarty, Antimony toxicity, International Journal of Environmental Research and Public Health. *7* (2010) 4267-77, doi:10.3390/ijerph7124267.

[3] S. Mohapatra, Drug resistance in leishmaniasis: Newer developments, Tropical Parasitology. 4 (2014) 4-9, doi:10.4103/2229-5070.129142.

[4] A. Taylor, Aminopeptidases: structure and function., The FASEB Journal : Official Publication of the Federation of American Societies for Experimental Biology. 7 (1993) 290–298, doi:10.1186/1750-1326-5-48.

[5] J. Timm, M. Valente, D. García-Caballero, K.S. Wilson, D. González-Pacanowska, Structural characterization of acidic M17 leucine aminopeptidases from the TriTryps and evaluation of their role in nutrient starvation in *Trypanosoma brucei*, mSphere. 2 (2017) e00226-17, doi:10.1128/mSphere.00226-17.

[6] U. Jankiewicz, W. Bielawski, The properties and functions of bacterial aminopeptidases, Acta Microbiologica Polonica. 52 (2003) 217-31.

[7] S.Y. Bhat, A. Dey, I.A. Qureshi, Structural and functional highlights of methionine aminopeptidase 2 from *Leishmania donovani*, International Journal of Biological Macromolecules. 115 (2018) 940–954, doi:10.1016/j.ijbiomac.2018.04.090.

[8] A. Addlagatta, X. Hu, J.O. Liu, B.W. Matthews, Structural basis for the functional differences between type I and type II human methionine aminopeptidases, Biochemistry. 44 (2005) 14741–14749, doi:10.1021/bi051691k.

[9] C. Giglione, A. Boularot, T. Meinnel, Protein N-terminal methionine excision, Cellular and Molecular Life Sciences. 61 (2004) 1455-74, doi:10.1007/s00018-004-3466-8.

[10] K.W. Walker, R.A. Bradshaw, Yeast methionine aminopeptidase I can utilize either

Zn2+ or Co2+ as a cofactor: a case of mistaken identity?, Protein Science : A Publication of the Protein Society. 7 (1998) 2684–7, doi:10.1002/pro.5560071224.

[11] G. Yang, R.B. Kirkpatrick, T. Ho, G.F. Zhang, P.H. Liang, K.O. Johanson, D.J. Casper, M.L. Doyle, J.P. Marino, S.K. Thompson, W. Chen, D.G. Tew, T.D. Meek, Steady-state kinetic characterization of substrates and metal-ion specificities of the full-length and N-terminally truncated recombinant human methionine aminopeptidases (Type 2), Biochemistry. 40 (2001) 10645–10654, doi:10.1021/bi010806r.

[12] L. Meng, S. Ruebush, V.M. D'souza, A.J. Copik, S. Tsunasawa, R.C. Holz, Overexpression and divalent metal binding properties of the methionyl aminopeptidase from *Pyrococcus furiosus*, Biochemistry. 41 (2002) 7199–7208, doi:10.1021/bi020138p.

[13] V.M. D'souza, R.C. Holz, The methionyl aminopeptidase from *Escherichia coli* can function as an iron(II) enzyme?, Biochemistry. 38 (1999) 11079-85, doi:10.1021/bi990872h.

[14] S. Liu, J. Widom, C.W. Kemp, C.M. Crews, J. Clardy, Structure of human methionine aminopeptidase-2 complexed with fumagillin., Science (New York, NY). 282 (1998) 1324–7, doi:10.1126/science.282.5392.1324.

[15] S.Y.P. Chang, E.C. McGary, S. Chang, Methionine aminopeptidase gene of *Escherichia coli* is essential for cell growth, Journal of Bacteriology. 171 (1989) 4071-2, doi:10.1128/jb.171.7.4071-4072.1989.

[16] X. Li, Y.H. Chang, Amino-terminal protein processing in *Saccharomyces cerevisiae* is an essential function that requires two distinct methionine aminopeptidases., Proceedings of the National Academy of Sciences. 92 (2006) 12357-61, doi:10.1073/pnas.92.26.12357.

[17] P.J. Rosenthal, Proteases of malaria parasites: New targets for chemotherapy, Emerging Infectious Diseases. 4 (1998) 49–57, doi:10.3201/eid0401.980107.

[18] F. Frottin, W. V. Bienvenut, J. Bignon, E. Jacquet, A. Sebastian Vaca Jacome, A. Van Dorsselaer, S. Cianferani, C. Carapito, T. Meinnel, C. Giglione, MetAP1 and MetAP2 drive cell selectivity for a potent anti-cancer agent in synergy, by controlling glutathione redox state, Oncotarget. 7 (2016) 63306-63323, doi:10.18632/oncotarget.11216.

[19] S.H. Chan, C.H. Chui, S.W. Chan, S.H.L. Kok, D. Chan, M.Y.T. Tsoi, P.H.M. Leung, A.K.Y. Lam, A.S.C. Chan, K.H. Lam, J.C.O. Tang, Synthesis of 8-hydroxyquinoline derivatives as novel antitumor agents, ACS Medicinal Chemistry Letters. 4 (2013) 170-4, doi:10.1021/ml300238z.

[20] M.P. Thakare, P. Kumar, N. Kumar, S.K. Pandey, Silica gel promoted environment-friendly synthesis of 2,3-disubstituted 4-thiazolidinones, Tetrahedron Letters. 55 (2014) 2463-66, doi:10.1016/j.tetlet.2014.03.007.

[21] X. Hu, A. Addlagatta, J. Lu, B.W. Matthews, J.O. Liu, Elucidation of the function of type 1 human methionine aminopeptidase during cell cycle progression, Proceedings of the National Academy of Sciences. 103 (2006) 18148-53, doi:10.1073/pnas.0608389103.

[22] R.C. Priest, J. Spaull, J. Buckton, R.L. Grimley, M. Sims, M. Binks, R. Malhotra, Immunomodulatory activity of a methionine aminopeptidase-2 inhibitor on B cell differentiation, Clinical and Experimental Immunology. 155 (2009) 514-22, doi:10.1111/j.1365-2249.2008.03843.x.

[23] N. Sin, L. Meng, M.Q.W. Wang, J.J. Wen, W.G. Bornmann, C.M. Crews, The anti-angiogenic agent fumagillin covalently binds and inhibits the methionine aminopeptidase, MetAP-2, Proceedings of the National Academy of Sciences. 94

(1997) 6099-6103, doi:10.1073/pnas.94.12.6099.

[24] X. Chen, C.R. Chong, L. Shi, T. Yoshimoto, D.J. Sullivan, J.O. Liu, Inhibitors of *Plasmodium falciparum* methionine aminopeptidase 1b possess antimalarial activity, Proceedings of the National Academy of Sciences of the United States of America. 103 (2006) 14548-53, doi:10.1073/pnas.0604101103.

[25] J.Y. Li, L.L. Chen, Y.M. Cui, Q.L. Luo, M. Gu, F.J. Nan, Q.Z. Ye, Characterization of full length and truncated type I human methionine aminopeptidases expressed from *Escherichia coli*, Biochemistry. 43 (2004) 7892-98, doi:10.1021/bi0360859.

[26] A. Marschner, C.D. Klein, Metal promiscuity and metal-dependent substrate preferences of *Trypanosoma brucei* methionine aminopeptidase 1, Biochimie. 115 (2015) 35–43, doi:10.1016/j.biochi.2015.04.012.

[27] R.G. Pearson, Acids and bases, Science. 151 (1966) 172-177, doi:10.1126/science.151.3707.172.

[28] Q.-Z. Ye, S.-X. Xie, Z.-Q. Ma, M. Huang, R.P. Hanzlik, Structural basis of catalysis by monometalated methionine aminopeptidase, Proceedings of the National Academy of Sciences of the United States of America. 103 (2006) 9470-75, doi:10.1073/pnas.0602433103.

[29] K.M. Hambidge, L. V. Miller, J.E. Westcott, X. Sheng, N.F. Krebs, Zinc bioavailability and homeostasis, American Journal of Clinical Nutrition. 91 (2010) 1478S-1483S, doi:10.3945/ajcn.2010.28674I.

[30] R.H. Holm, P. Kennepohl, E.I. Solomon, Structural and functional aspects of metal sites in biology, Chemical Reviews. 96 (1996) 2239-2314, doi:10.1021/cr9500390.

[31] A. Addlagatta, B.W. Matthews, Structure of the angiogenesis inhibitor ovalicin bound to its noncognate target, human type 1 methionine aminopeptidase, Protein Science. 15 (2006) 1842-1848, doi:10.1110/ps.062278006.

[32] S.S.Kerwar, H. Weissbach, G.G. Glenner, An aminopeptidase activity associated with brain ribosomes, Archives of Biochemistry and Biophysics. 143 (1971) 336-7, doi: 10.1016/0003-9861(71)90215-3

[33] V. Kumar, N. Sharma, T.C. Bhalla, In silico analysis of β-galactosidases primary and secondary structure in relation to temperature adaptation, Journal of Amino Acids. 2014 (2014) 475839, doi:10.1155/2014/475839.

[34] S. Swallow, Fluorine in medicinal chemistry, in: Progress in Medicinal Chemistry. 54 (2015) 65-133, doi:10.1016/bs.pmch.2014.11.001.

[35] I. Letunic, P. Bork, 20 years of the SMART protein domain annotation resource, Nucleic Acids Research. 46 (2018) D493-96, doi:10.1093/nar/gkx922.

[36] A. Sali, MODELLER A Program for Protein Structure Modeling Release 9v4, r6262, http://salilab.org/modeller/.

[37] D. Van Der Spoel, E. Lindahl, B. Hess, G. Groenhof, A.E. Mark, H.J.C. Berendsen, GROMACS: Fast, flexible, and free, Journal of Computational Chemistry. 26 (2005) 1701–1718, doi:10.1002/jcc.20291.

[38] W. Wang, M. Xia, J. Chen, F. Deng, R. Yuan, X. Zhang, F. Shen, Data set for phylogenetic tree and RAMPAGE Ramachandran plot analysis of SODs in *Gossypium raimondii* and *G. arboreum*, Data in Brief. 9 (2016) 345–348, doi:10.1016/j.dib.2016.05.025.

[39] W.L. DeLano, The PyMOL Molecular Graphics System, Schrödinger LLC wwwpymolorg. Version 1. (2002) http://www.pymol.org. doi:citeulike-article-id:240061.

[40] A. Daina, O. Michielin, V. Zoete, SwissADME: A free web tool to evaluate pharmacokinetics, drug-likeness and medicinal chemistry friendliness of small molecules, Scientific Reports. 3 (2017). doi:10.1038/srep42717.

[41] P. Alam, A.S. Abdelhameed, R.K. Rajpoot, R.H. Khan, Interplay of multiple interaction forces: Binding of tyrosine kinase inhibitor nintedanib with human serum albumin, Journal of Photochemistry and Photobiology B: Biology. 157 (2016) 70–76, doi:10.1016/j.jphotobiol.2016.02.009.

[42] O. Trott, A.J. Olson, AutoDock Vina: improving the speed and accuracy of docking with a new scoring function, efficient optimization, and multithreading, Journal of Computational Chemistry. 31 (2010) 445–461, doi:10.1002/jcc.21334.

[43] D.M.F. van Aalten, R. Bywater, J.B.C. Findlay, M. Hendlich, R.W.W. Hooft, G. Vriend, PRODRG, a program for generating molecular topologies and unique molecular descriptors from coordinates of small molecules, Journal of Computer-Aided Molecular Design. 10 (1996) 255–262, doi:10.1007/BF00355047.

Tables

Table 1. Steady-state kinetic parameters of *Ld*MetAP1 with metal chlorides against L-methionine-4-methyl-coumaryl-7-amide. Data represents mean ± SD from three experiments.

Metal	**K_m (µM)**	**k_{cat}(min^{-1})**	**$k_{cat}/K_m \times 10^3$ ($M^{-1}min^{-1}$)**
$FeCl_2$	40.36 ± 5.43	4.63 ± 0.21	114.71 ± 16.28
$CoCl_2$	111.2 ± 7.01	7.52 ± 0.23	67.62 ± 4.73
$MnCl_2$	145.5 ± 11.80	6.07 ± 0.27	41.71 ± 3.85
$MgCl_2$	95.88 ± 10.87	2.24 ± 0.12	23.36 ± 2.92
$CaCl_2$	244.7 ± 48.15	2.79 ± 0.43	11.40 ± 2.84

Table 2. IC_{50} values of HQ1-HQ20 against *Ld*MetAP1 and its human ortholog *Hs*MetAP1

Compound	***Ld*MetAP1 IC_{50} (µM)**	***Hs*MetAP1 IC_{50} (µM)**
HQ1	251.6	very far
HQ2	62.5	104.7
HQ3	39.71	very far
HQ4	45.49	143
HQ5	79.87	116.1
HQ6	46.36	very far
HQ7	54.10	107
HQ8	26.44	10.94
HQ9	12.94	61.4
HQ10	18.42	12.58
HQ11	8.80	8.90
HQ12	18.42	98.70
HQ13	11.70	217.2

HQ14	1.31	very far
HQ15	1.10	284.0
HQ16	43.80	127.5
HQ17	36.77	104.2
HQ18	46.14	112.7
HQ19	37.38	174.6
HQ20	27.91	126.8

Table 3. Predicted ADME properties of hit compounds and cell viability analysis for assessing toxicity.

Compound	**MW (g/mol)**	**LogP**	**LogS**	**Pharmacokinetics**	**Drug likeness**	**Cytotoxicity (IC_{50})**
HQ11	340.37	2.93	-4.46	High	Yes	~ 120 μM
HQ13	347.39	2.76	-4.24	High	Yes	> 250 μM
HQ14	336.41	2.99	-4.60	High	Yes	> 200 μM
HQ15	356.83	3.08	-4.90	High	Yes	>200 μM

Table 4. Equilibrium dissociation constants (K_D) of *Ld*MetAP1 and *Hs*MetAP1 with hit compounds. Data represents mean of two independent experiments.

Enzyme	**Analyte**	**K_D (M)**
*Ld*MetAP1	HQ-11	1.61×10^{-10}
*Ld*MetAP1	HQ-13	1.54×10^{-8}
*Ld*MetAP1	HQ-14	2.15×10^{-8}
*Ld*MetAP1	HQ-15	1.50×10^{-8}
*Hs*MetAP1	HQ-11	1.52×10^{-10}
*Hs*MetAP1	HQ-13	3.53×10^{-8}
*Hs*MetAP1	HQ-14	8.52×10^{-8}
*Hs*MetAP1	HQ-15	3.61×10^{-7}

Table 5. Percentage yield of Compounds 4 (HQ1-20)

S. No	**Compound**	**R**	**Yield %***
1	HQ1	4-I	68
2	HQ2	4-OCH_3	65
3	HQ3	3-OCH_3	70
4	HQ4	4-F	70
5	HQ5	4-H	72
6	HQ6	3-OCF_3	70
7	HQ7	4CF_3	69
8	HQ8	3,4(di)OCH_3	65
9	HQ9	3,4,5(tri)OCH_3	69
10	HQ10	3,5(di)OCH_3	60
11	HQ11	3-F	65
12	HQ12	2-OCH_3	67
13	HQ13	3-CN	70
14	HQ14	4-CH_3	72

15	HQ15	4-Cl	80
16	HQ16	4-OPh	73
17	HQ17	4-Br	72
18	HQ18	3-Br	70
19	HQ19	4-$CH(CH_3)_2$	70
20	HQ20	3-CH_3	74

*****Yield % is the isolated yield

Figure legends

Fig. 1: Chemical structures of 8-Hydroxyquinoline-substituted 4-Thiazolidinones [**4** (HQ1-HQ20)].

Fig. 2: Domain organisation, sequence analysis and purification. (A) Domain architecture of *Ld*MetAP1 showing its two domains. NTD (grey) and CTCD (blue) stand for N-terminal domain and C-terminal catalytic domain, respectively. (B) Modelled structure of *Ld*MetAP1 depicting the pita-bread fold organization typical of MetAPs. Helices are shown in olive, sheets in blue and loops in black. Green spheres display the two divalent metal ions requisite for catalysis. (C) LigPlot showing the metal interacting residues DDHEE of *Ld*MetAP1. Residues are numbered according to the full length sequence of *Ld*MetAP1 (D) Multiple sequence alignment of *Ld*MetAP1 with its ortholog sequences from *T. brucei* and *H. sapiens.* Secondary structure found in the modelled structure of *Ld*MetAP1 is highlighted. Conserved and similar residues are shown in red and yellow colour, respectively. Blue stars indicate conserved catalytic metal interacting residues. (E) Purification of recombinant *Ld*MetAP1 (lane 1 and 2) and mutazyme T291A (lane 3 and 4). (F) Purification of *Hs*MetAP1 (lane 1 and 2). Lane M represents the pre-stained marker. (G) Gel filtration chromatogram of *Ld*MetAP1 highlighting the monomeric state of this enzyme in solution.

Fig. 3: Biophysical and biochemical characterization of *Ld*MetAP1. (A) Far-UV CD spectra of *Ld*MetAP1 and mutazyme T291A. (B) Heat-denaturation plots of *Ld*MetAP1 and T291A. (C) Michaelis-Menten fit for the aminopeptidase activity of *Ld*MetAP1 with different metal chlorides. (D) Relative activity of *Ld*MetAP1 against different peptide substrates. Data indicates mean ± SD of three experiments.

Fig. 4: Inhibition of aminopeptidase activity of *Ld*MetAP1 and *Hs*MetAP1. (A-D) Differential inhibition of *Ld*MetAP1 and *Hs*MetAP1 with inhibitors HQ11, HQ13, HQ14 and HQ15. (E) Lineweaver-Burk plots depicting the uncompetitive mode of inhibition of HQ11.

Figures (F-H) depict the competitive mode of inhibition of HQ13, HQ14 and HQ15. Data indicates mean ± SD of four experiments performed in triplicates.

Fig. 5: Binding interaction of *Ld*MetAP1 and *Hs*MetAP1 with inhibitors. (A-D) SPR sensorgrams showing binding interaction between *Ld*MetAP1 and inhibitors HQ11, HQ13, HQ14 and HQ15. (E-H) Binding interactions of *Hs*MetAP1 with inhibitors. The data presented is a mean of two independent experiments performed at room temperature.

Fig. 6: Biochemical digressions after mutagenesis and molecular docking. (A) Plot showing the high catalytic efficiency of *Ld*MetAP1 over mutazymeT291A. Statistical analysis was performed with two-tailed student's t-test. Catalytic efficiency was considered statistically significant when $P< 0.05$. (B-D) Differential inhibition of *Ld*MetAP1 with specific inhibitors HQ13, HQ14 and HQ15 after mutation of Thr291 to Ala. Data indicates mean ± SD of three experiments performed in triplicates. (E-G) Rotameric flipping of residues surrounding the active site after mutation of Thr291 to either Ala (F) or Val (G) and atomic interactions of HQ15 with *Ld*MetAP1 and mutazymes T291A and T291V. HQ15 and interacting residues are given in sticks. Discontinuous black lines in the figure display hydrogen bonding. Other residues shown in the figures in sticks have hydrophobic interactions with HQ15.

Fig. 7: Structural basis of inhibition. (A-D) LigPlots showing the hydrogen bonding and hydrophobic interactions of inhibitors with *Ld*MetAP1. (E-H) LigPlot analysis displaying the inhibitor interactions with *Hs*MetAP1. Structures of *Ld*MetAP1 and *Hs*MetAP1 are shown as a surface with binding poses of HQ11 (black sticks), HQ13 (Red sticks), HQ14 (cyan sticks) and HQ15 (blue sticks).

Fig. 8: Molecular dynamics. Figures **(**A), (B) and (C) show the group parameters RMSD, RMSF and Rg of *Ld*MetAP1, T291A and their complexes with lead inhibitor HQ15.

Supplementary figure legends

Supplementary Fig. 1: (A) Effect of varying pH on the amidolytic activity of *Ld*MetAP1. (B) Inhibition of *Ld*MetAP1 with HQ1 and HQ4 molecules. Data indicates mean ± SD of three experiments.

Supplementary Fig. 2: (A-L) Fluorescence spectra, Stern-Volmer plots and modified Stern-Volmer plots of *Ld*MetAP1 with inhibitors HQ11, HQ13, HQ14 and HQ15.

Supplementary Fig. 3: (A-B) Non-linear regression fit for the determination of inhibition constant (K_i) of HQ13, HQ14 and HQ15 with *Ld*MetAP1 and mutazyme T291A. The parameters highlight high affinity and potency of lead molecules for *Ld*MetAP1. Data indicates mean ± SD of two experiments performed in triplicates.

Figure 1

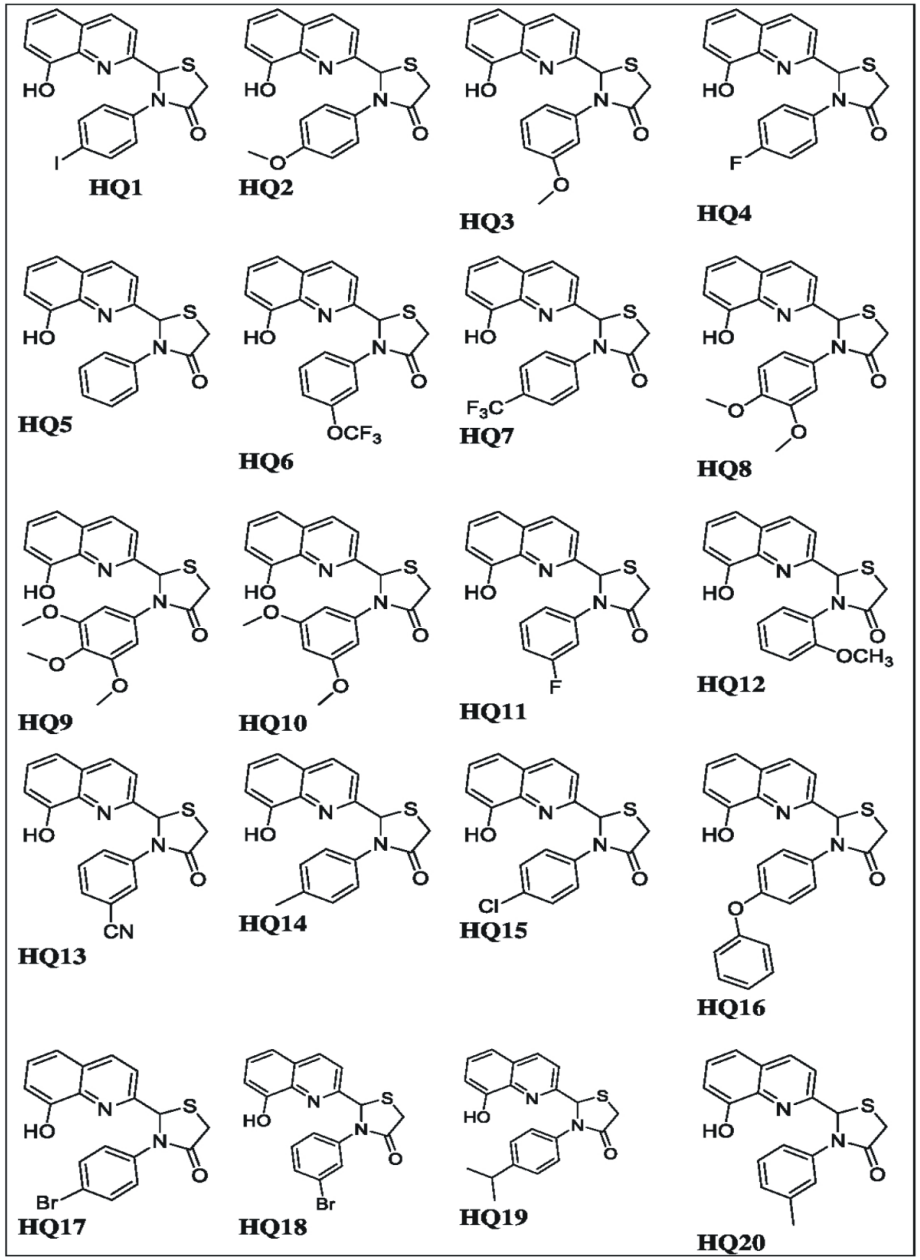
HQ1
HQ2
HQ3
HQ4
HQ5
HQ6
HQ7
HQ8
HQ9
HQ10
HQ11
HQ12
HQ13
HQ14
HQ15
HQ16
HQ17
HQ18
HQ19
HQ20

Figure 2

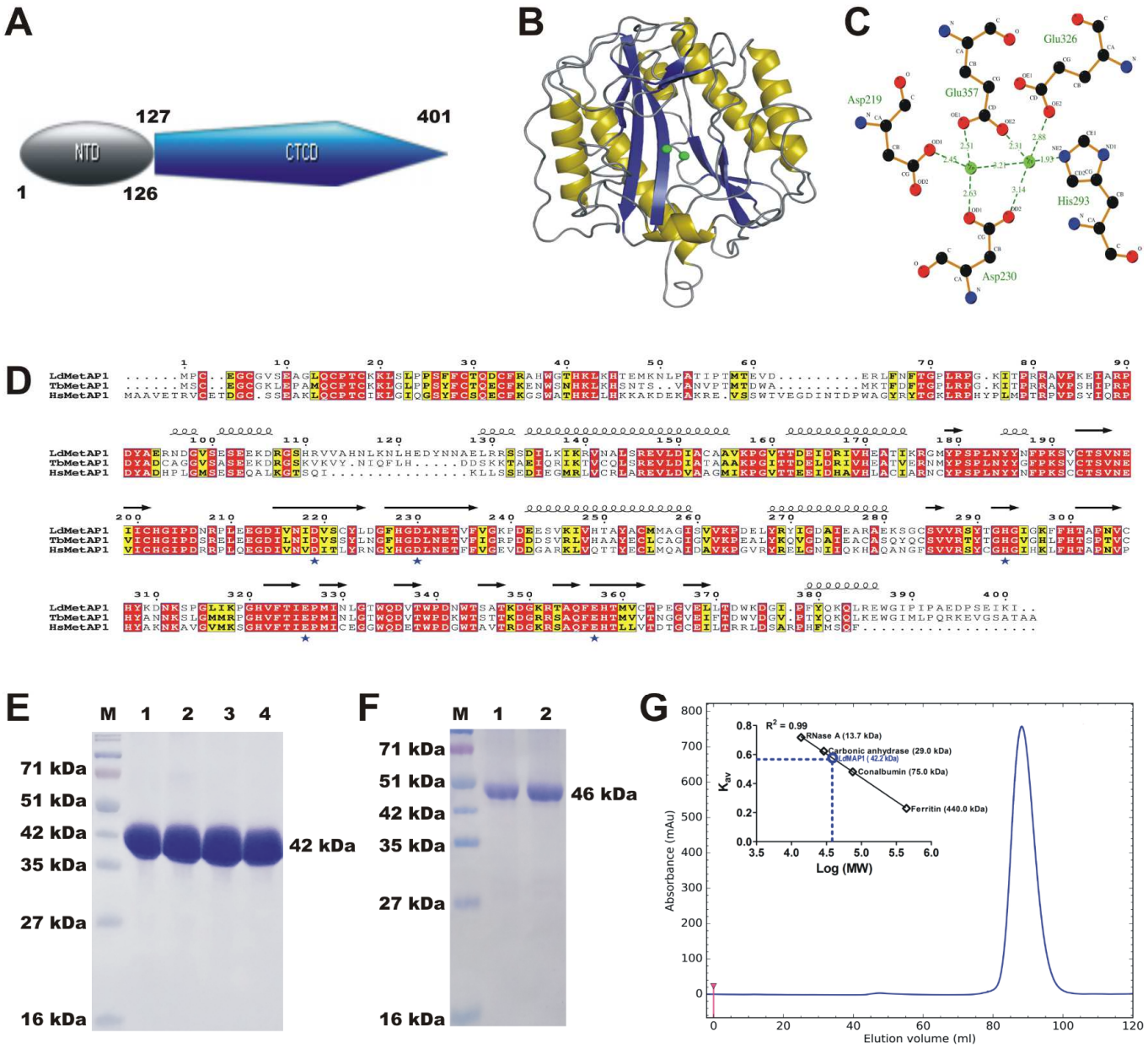
A
127
401
NTD
CTCD
1
126
B
C
Glu326
Asp219
Glu357
His293
Asp230
D
LdMetAP1
TbMetAP1
HsMetAP1
E
M 1 2 3 4
71 kDa
51 kDa
42 kDa
35 kDa
27 kDa
16 kDa
42 kDa
F
M 1 2
71 kDa
51 kDa
42 kDa
35 kDa
27 kDa
16 kDa
46 kDa
G
R² = 0.99
RNase A (13.7 kDa)
Carbonic anhydrase (29.0 kDa)
LdMAP1 (42.2 kDa)
Conalbumin (75.0 kDa)
Ferritin (440.0 kDa)
Kav
Log (MW)
Absorbance (mAu)
Elution volume (ml)

Figure 3

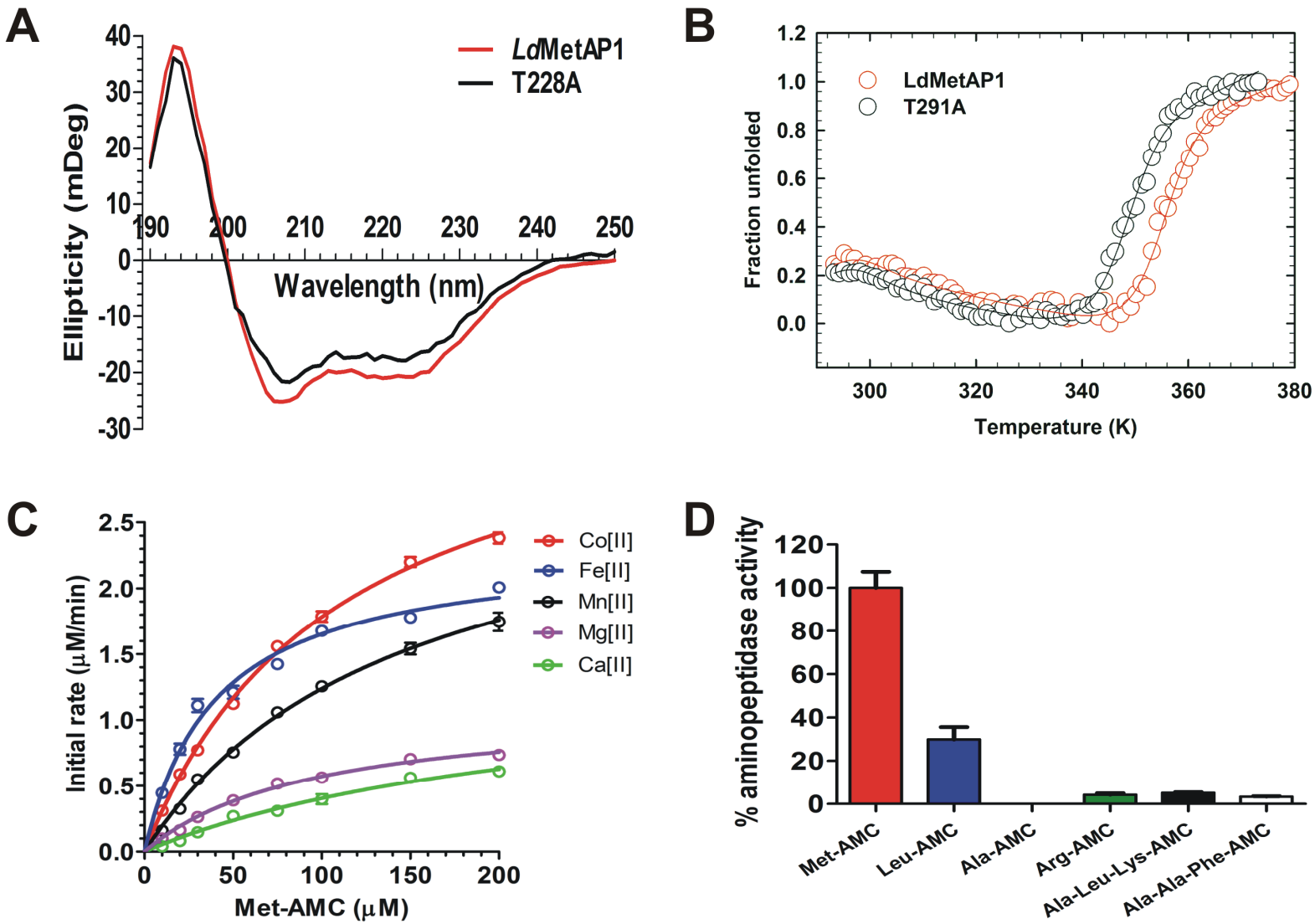
A
LdMetAP1
T228A
Ellipticity (mDeg)
Wavelength (nm)
B
LdMetAP1
T291A
Fraction unfolded
Temperature (K)
C
Co[II]
Fe[II]
Mn[II]
Mg[II]
Ca[II]
Initial rate (μM/min)
Met-AMC (μM)
D
% aminopeptidase activity
Met-AMC
Leu-AMC
Ala-AMC
Arg-AMC
Ala-Leu-Lys-AMC
Ala-Ala-Phe-AMC

Figure 4

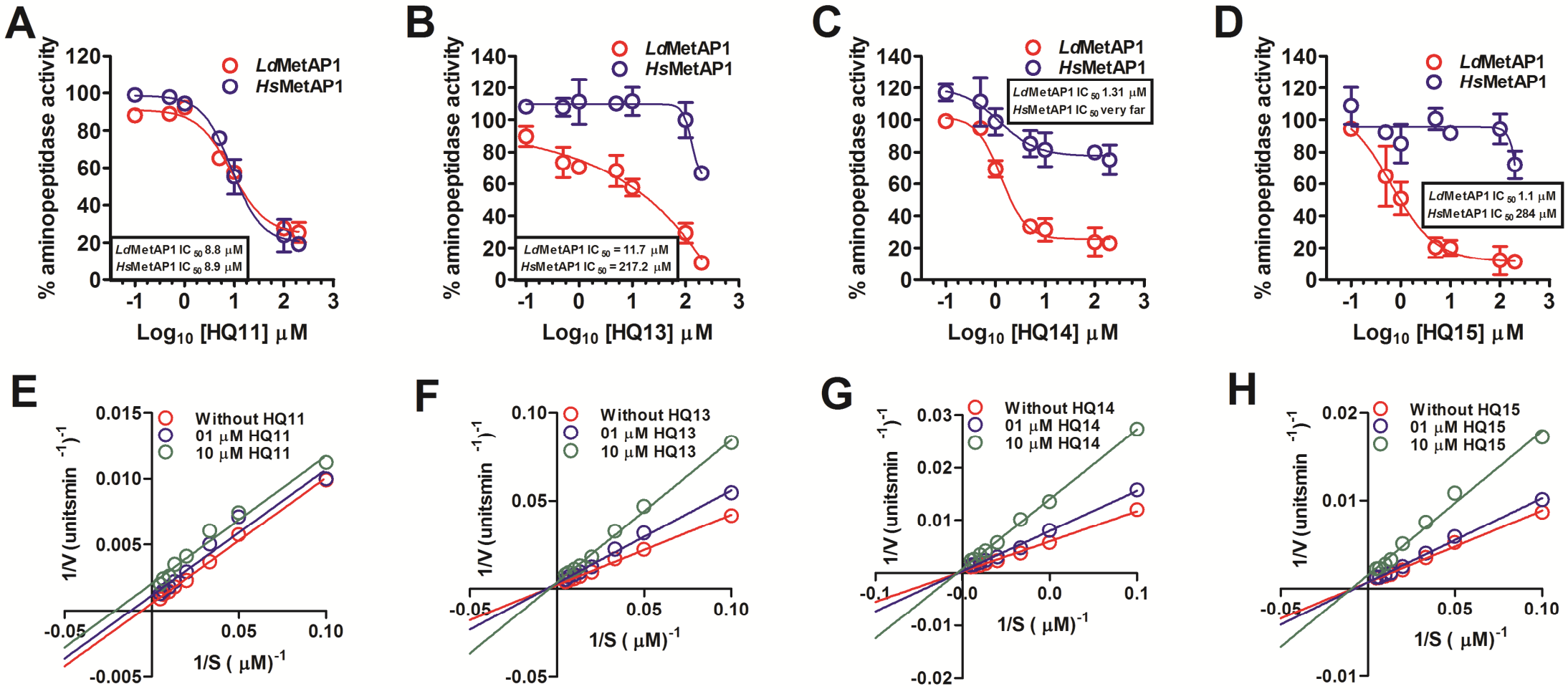
A
% aminopeptidase activity
LdMetAP1
HsMetAP1
LdMetAP1 IC50 8.8 µM
HsMetAP1 IC50 8.9 µM
Log10 [HQ11] µM
B
% aminopeptidase activity
LdMetAP1
HsMetAP1
LdMetAP1 IC50 = 11.7 µM
HsMetAP1 IC50 = 217.2 µM
Log10 [HQ13] µM
C
% aminopeptidase activity
LdMetAP1
HsMetAP1
LdMetAP1 IC50 1.31 µM
HsMetAP1 IC50 very far
Log10 [HQ14] µM
D
% aminopeptidase activity
LdMetAP1
HsMetAP1
LdMetAP1 IC50 1.1 µM
HsMetAP1 IC50 284 µM
Log10 [HQ15] µM
E
1/V (unitsmin -1)-1
Without HQ11
01 µM HQ11
10 µM HQ11
1/S (µM)-1
F
1/V (unitsmin -1)-1
Without HQ13
01 µM HQ13
10 µM HQ13
1/S (µM)-1
G
1/V (unitsmin -1)-1
Without HQ14
01 µM HQ14
10 µM HQ14
1/S (µM)-1
H
1/V (unitsmin -1)-1
Without HQ15
01 µM HQ15
10 µM HQ15
1/S (µM)-1

Figure 5

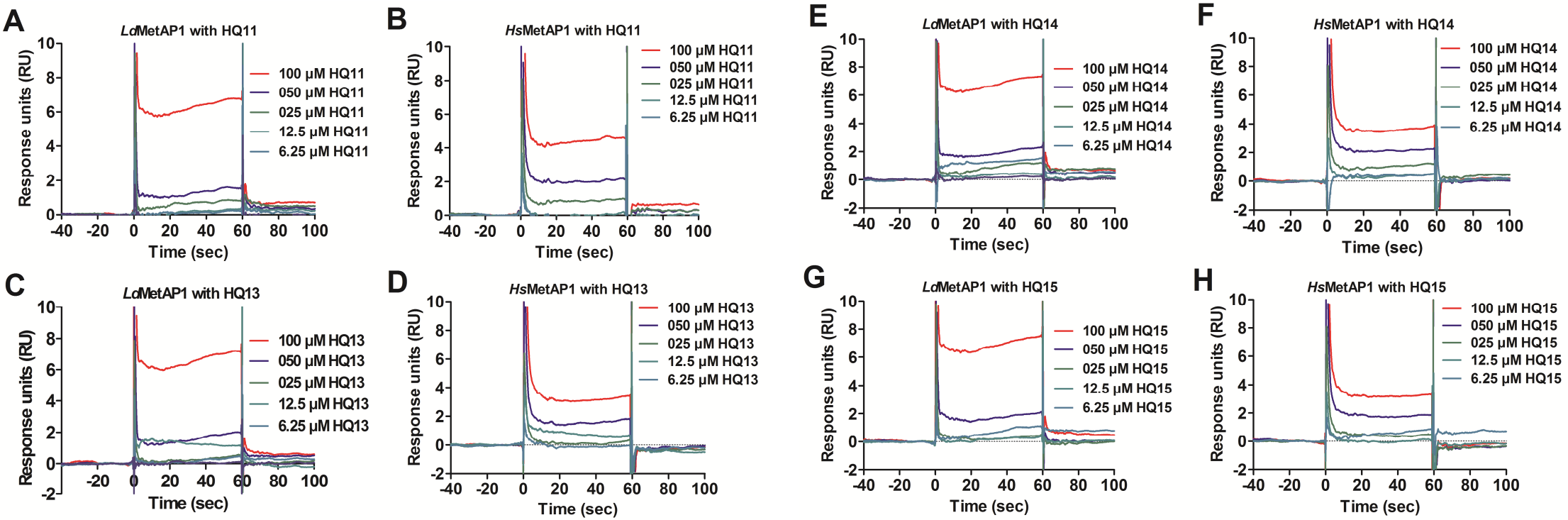
A
LdMetAP1 with HQ11
100 µM HQ11
050 µM HQ11
025 µM HQ11
12.5 µM HQ11
6.25 µM HQ11
B
HsMetAP1 with HQ11
100 µM HQ11
050 µM HQ11
025 µM HQ11
12.5 µM HQ11
6.25 µM HQ11
C
LdMetAP1 with HQ13
100 µM HQ13
050 µM HQ13
025 µM HQ13
12.5 µM HQ13
6.25 µM HQ13
D
HsMetAP1 with HQ13
100 µM HQ13
050 µM HQ13
025 µM HQ13
12.5 µM HQ13
6.25 µM HQ13
E
LdMetAP1 with HQ14
100 µM HQ14
050 µM HQ14
025 µM HQ14
12.5 µM HQ14
6.25 µM HQ14
F
HsMetAP1 with HQ14
100 µM HQ14
050 µM HQ14
025 µM HQ14
12.5 µM HQ14
6.25 µM HQ14
G
LdMetAP1 with HQ15
100 µM HQ15
050 µM HQ15
025 µM HQ15
12.5 µM HQ15
6.25 µM HQ15
H
HsMetAP1 with HQ15
100 µM HQ15
050 µM HQ15
025 µM HQ15
12.5 µM HQ15
6.25 µM HQ15
Response units (RU)
Time (sec)

Figure 6

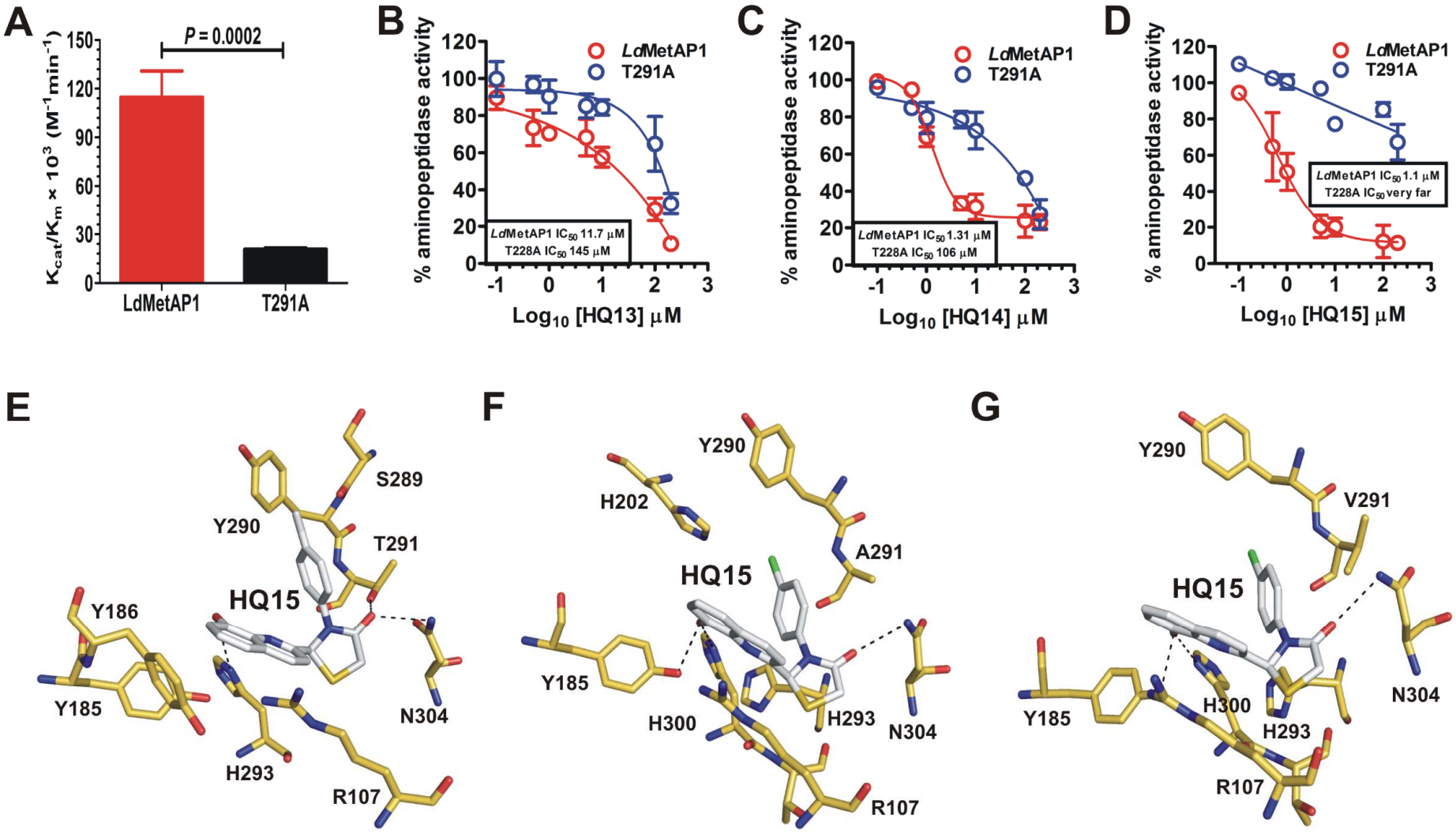
A
P = 0.0002
$K_{cat}/K_m \times 10^3$ ($M^{-1}min^{-1}$)
LdMetAP1
T291A
B
% aminopeptidase activity
LdMetAP1
T291A
LdMetAP1 IC50 11.7 µM
T228A IC50 145 µM
Log10 [HQ13] µM
C
% aminopeptidase activity
LdMetAP1
T291A
LdMetAP1 IC50 1.31 µM
T228A IC50 106 µM
Log10 [HQ14] µM
D
% aminopeptidase activity
LdMetAP1
T291A
LdMetAP1 IC50 1.1 µM
T228A IC50 very far
Log10 [HQ15] µM
E
S289
Y290
T291
HQ15
Y186
Y185
N304
H293
R107
F
Y290
H202
A291
HQ15
Y185
H300
H293
N304
R107
G
Y290
V291
HQ15
N304
Y185
H300
H293
R107

Figure 7

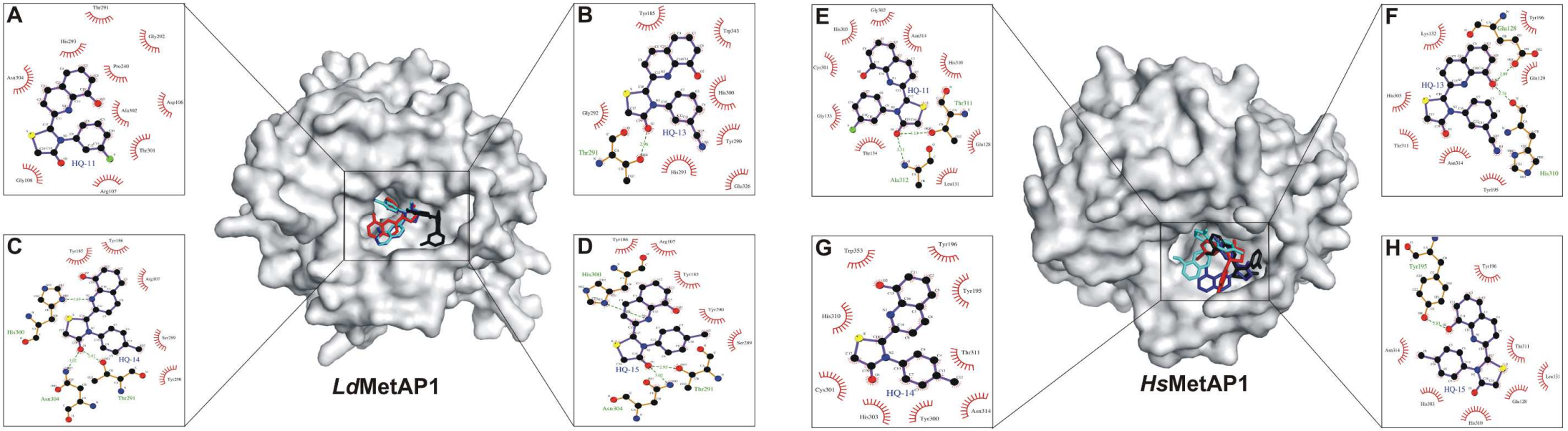

Figure 8

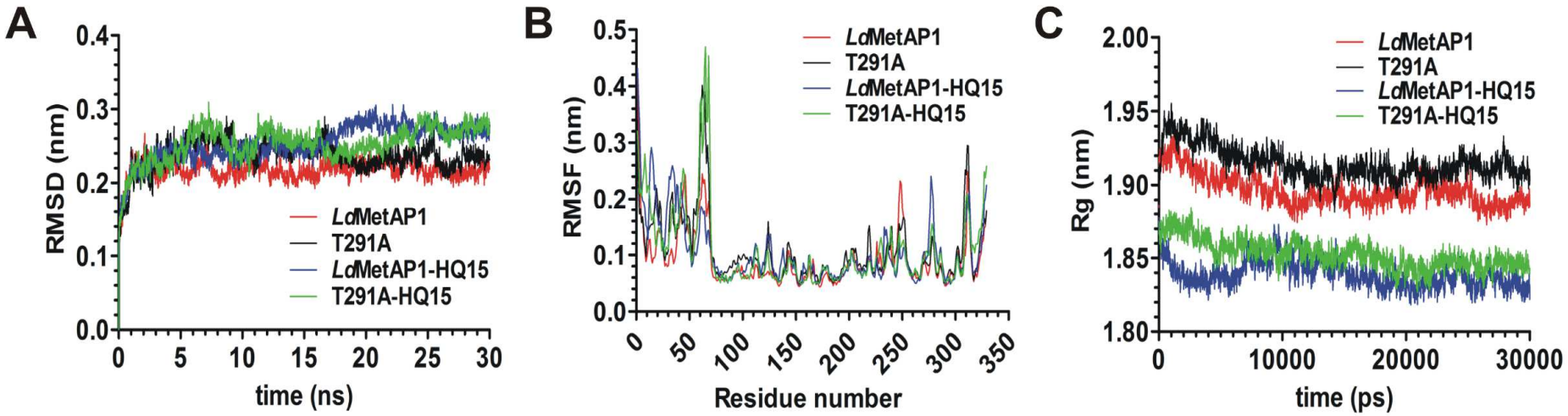
A
RMSD (nm)
0.0
0.1
0.2
0.3
0.4
0
5
10
15
20
25
30
time (ns)
LdMetAP1
T291A
LdMetAP1-HQ15
T291A-HQ15
B
RMSF (nm)
0.0
0.1
0.2
0.3
0.4
0.5
0
50
100
150
200
250
300
350
Residue number
LdMetAP1
T291A
LdMetAP1-HQ15
T291A-HQ15
C
Rg (nm)
1.80
1.85
1.90
1.95
2.00
0
10000
20000
30000
time (ps)
LdMetAP1
T291A
LdMetAP1-HQ15
T291A-HQ15

Supplementary Figure 1

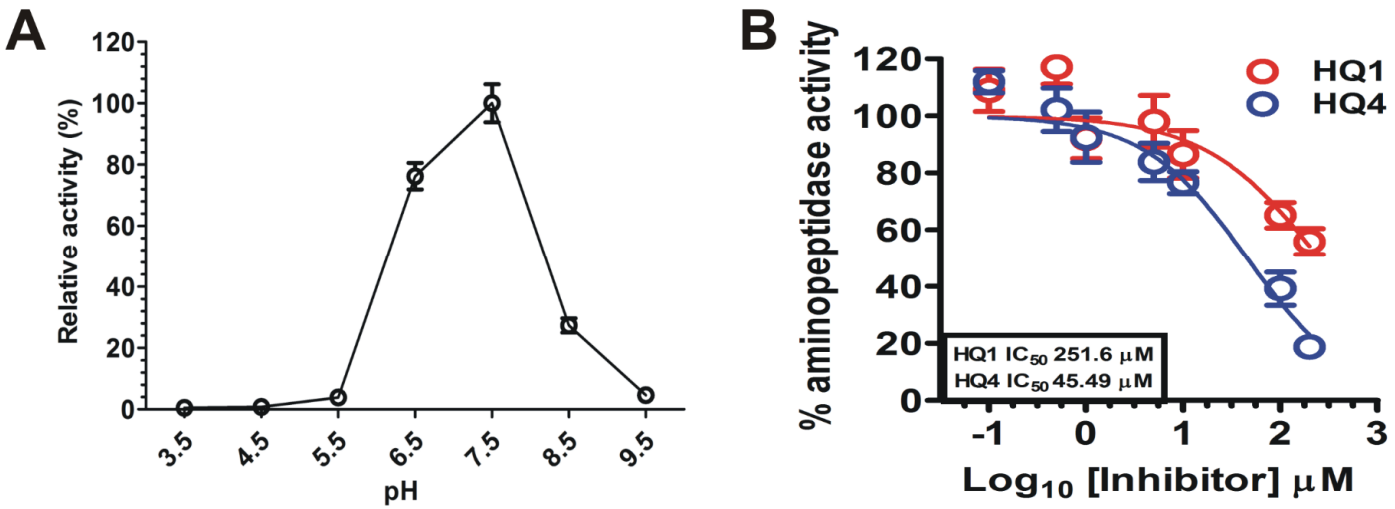

Supplementary Figure 2

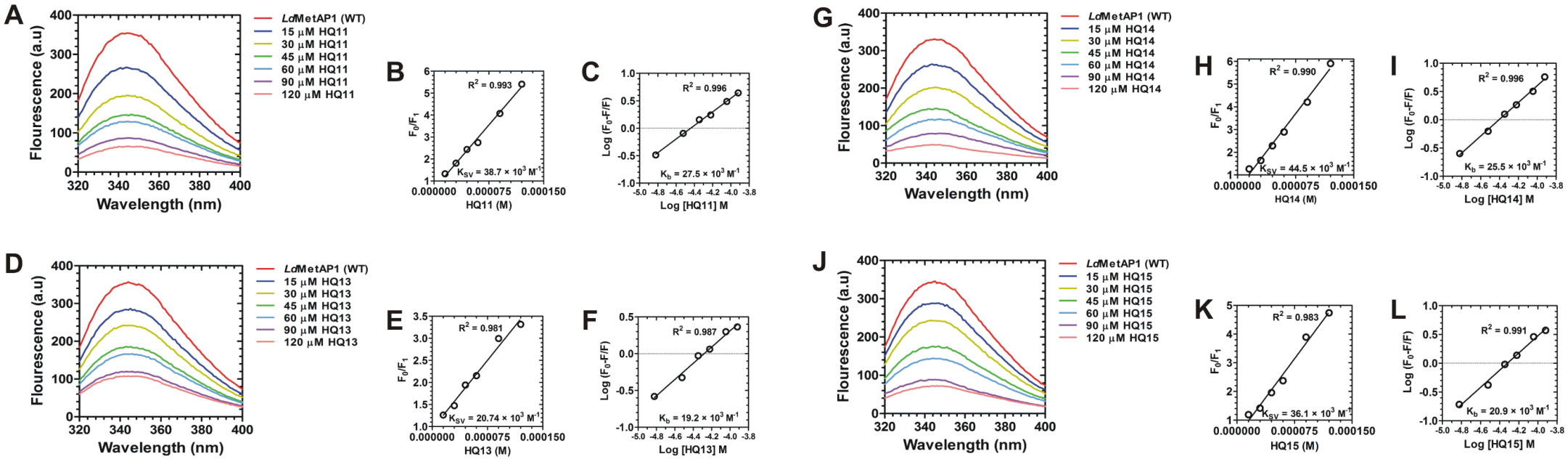

Supplementary Figure 3

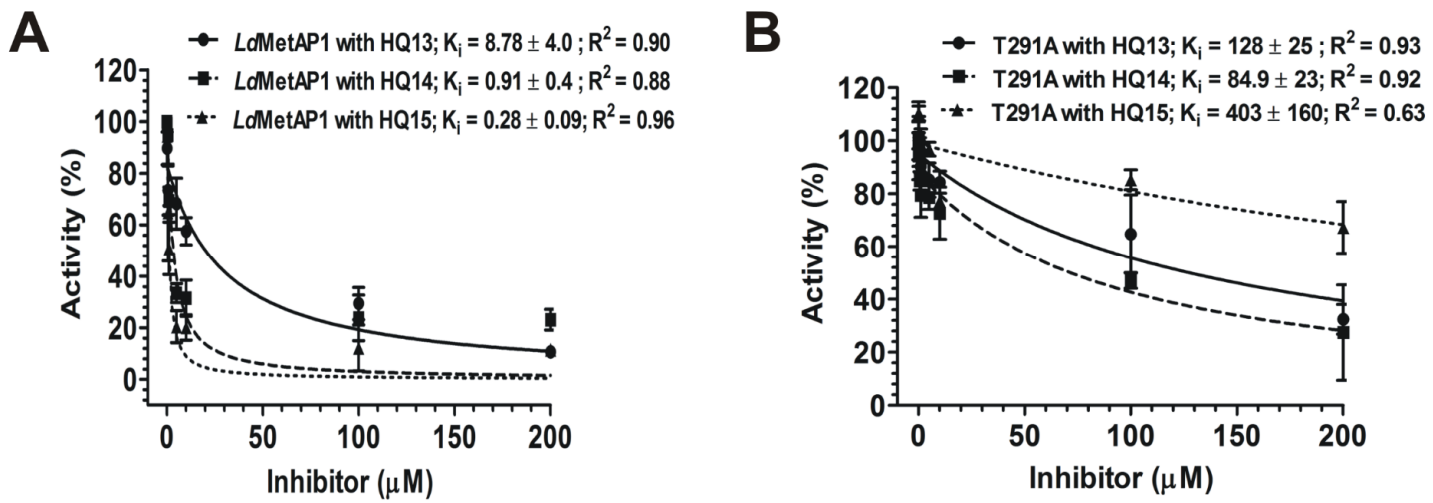

Highlights

- Leishmanial methionine aminopeptidase (*Ld*MetAP1) is a monomeric metal dependent methionine excising enzyme.
- Unlike its human counterpart, *Ld*MetAP1 is potently inhibited by two quinoline-carbaldehyde derivatives (HQ14 and HQ15).
- Specific inhibitors HQ14 and HQ15 inhibit *Ld*MetAP1 competitively and exhibit high-order binding along with druglikeness.
- Different amino acid composition of *Ld*MetAP1 and *Hs*MetAP1 near the conserved catalytic site provides structural basis of inhibition.